Naval Research Laboratory
Washington, DC 20375-5320

NRL/6120/MR—2022/2

Metal-Organic Frameworks as Sorbents of Perfluoroalkyl Substances and their Reduction by the Hydrated Electron

WILLIAM MAZA

Materials Chemistry and Dynamics Branch
Chemistry Division

February 10, 2022

REPORT DOCUMENTATION PAGE

Form Approved
OMB No. 0704-0188

1. REPORT DATE *(DD-MM-YYYY)*	**2. REPORT TYPE**	**3. DATES COVERED** *(From - To)*
10-02-2022	NRL Memorandum Report	11/19/2019 – 11/19/2020

4. TITLE AND SUBTITLE

Metal-Organic Frameworks as Sorbents of Perfluoroalkyl Substances and their Reduction by the Hydrated Electron

5a. CONTRACT NUMBER

5b. GRANT NUMBER

5c. PROGRAM ELEMENT NUMBER
NISE

6. AUTHOR(S)

William Maza

5d. PROJECT NUMBER

5e. TASK NUMBER

5f. WORK UNIT NUMBER
N2V5

7. PERFORMING ORGANIZATION NAME(S) AND ADDRESS(ES)

Naval Research Laboratory
4555 Overlook Avenue, SW
Washington, DC 20375-5320

8. PERFORMING ORGANIZATION REPORT NUMBER

NRL/6120/MR--2022/2

9. SPONSORING / MONITORING AGENCY NAME(S) AND ADDRESS(ES)

Naval Research Laboratory
4555 Overlook Avenue, SW
Washington, DC 20375-5320

10. SPONSOR / MONITOR'S ACRONYM(S)
NRL-NISE

11. SPONSOR / MONITOR'S REPORT NUMBER(S)

12. DISTRIBUTION / AVAILABILITY STATEMENT

DISTRIBUTION STATEMENT A: Approved for public release; distribution is unlimited.

13. SUPPLEMENTARY NOTES
Karles Fellowship

14. ABSTRACT

The rising environmental footprint of perfluoroalkyl substances and other anionic contaminants necessitates the development of technologies that are safe and efficient at remediating contaminated waters. In this memorandum report, the sequestration of negatively charged contaminants, including PFAS, by metal-organic frameworks and the reduction of PFAS by the hydrated electron are investigated.

15. SUBJECT TERMS

Metal-organic frameworks MOF Perfluoroalkyl substances PFAS Perfluorooctanoate PFOA
Perfluorooctane sulfonate PFOS Sulfite Ferrocyanide Hydrated electron

16. SECURITY CLASSIFICATION OF:			**17. LIMITATION OF ABSTRACT**	**18. NUMBER OF PAGES**	**19a. NAME OF RESPONSIBLE PERSON**
					William Maza
a. REPORT	**b. ABSTRACT**	**c. THIS PAGE**	U	31	**19b. TELEPHONE NUMBER** *(include area code)*
U	U	U			(202) 404-1648

This page intentionally left blank.

CONTENTS

FIGURES

and $K_4Fe(CN)_6$ are 9.1 ± 0.2 μs and 7.4 ± 0.2 μs, respectively. (Right panel) Lifetime of the photodetached e_{aq}^- as a function of pH in solutions of 10 mM Na_2SO_3 (open black circles) and 40 μM $K_4Fe(CN)_6$ (open red circles). Solid lines represent best fits of the data to equations **8a** and **9**, respectively.

Figure 11. (Left panel) Overlay of the experimentally determined e_{aq}^- lifetimes (open circles) and predicted concentrations of $Fe(CN)_6^{4-}$ (dashed line) and $Fe(CN)_5(HCN)^{3-}$ based on the reported pK_a of 4.1 in a 40 μM solution of $K_4Fe(CN)_6$ as a function of pH. (Right panel) Overlay of the same experimentally determined e_{aq}^- lifetimes (black open circles) in a 40 μM solution of $K_4Fe(CN)_6$ as a function of pH and the predicted lifetimes (solid lines) computed using equation **9** in the main text as a function of pH by varying the magnitude of k_2 and k_3 where $[Fe(CN)_6^{4-}]_o$ was fixed at 40 μM (Black line: k2 = $3x10^9$ M^{-1} s^{-1}, k3 = $2.3x10^{10}$ M^{-1} s^{-1}; Red line: k2 = 0, k3 = $2.3x10^{10}$ M^{-1} s^{-1}; Blue line: k2 = 0, k3 = $9.8x10^9$ M^{-1} s^{-1}; Green line: k2 = $3x10^9$ M^{-1} s^{-1}, k3 = $9.8x10^9$ M^{-1} s^{-1}).

Figure 12. **(**Left panel, top) Transient absorption decay traces of e_{aq}^- obtained at 790 nm in a 40 μM $K_4Fe(CN)_6$ solution in the absence (black) and presence (red) of 40 μM PFOS at pH 8. (Left panel, bottom) Transient absorption decay traces of e_{aq}^- obtained at 790 nm in a 10 mM Na_2SO_3 solution in the absence (black) and presence (red) of 40 μM PFOS at pH 9. (Right panel) Stern-Volmer analysis of e_{aq}^- quenching in 10 mM Na_2SO_3 solutions at pH 9 (red open circles) and 40 μM $K_4Fe(CN)_6$ solutions at pH 8 (black open circles).

Figure 13. (Left panel) Normalized transient e_{aq}^- lifetime decays in the absence (black) and presence of 230 μM PF8S (red) and 280 μM PF8A (blue). (Right panel) Plot of the k_q for the various PFxAs (blue) and PFxSs (red) probed here as a function of the number of perfluorinated carbons in the PFAS backbone.

Figure 14. (Left panel) Stern-Volmer plots for the quenching of e_{aq}^- by PF9A (red), PF8A (blue), PF7A (green), PF6A (purple), PF5A (orange), PF4A (brown), PF3A (light blue), and PF2A (cyan). (Right panel) Stern-Volmer plots for the quenching of e_{aq}^- by PF8S (red), PF6S (blue), and PF4S (green).

Figure 15. Arrhenius plots for the temperature dependence on the quenching rate constant, k_q, for (left panel) PFxA and (right panel) PFxS.

Figure 16. Activation energies for the reduction of PFxA (black squares) and PFxS (red circles) as a function of the number of fluorinated carbons comprising the fluoroalkyl backbone.

TABLES

Table 1. Bimolecular quenching rate constant and activation energy for the reaction between e_{aq}^- and PFxA, PFxS.

This page intentionally left blank.

EXECUTIVE SUMMARY

The rising environmental footprint of perfluoroalkyl substances (PFASs) and other anionic contaminants necessitates the development of technologies that are safe and efficient at remediating contaminated waters. In this memorandum report, the sequestration of negatively charged contaminants, including PFAS, by metal-organic frameworks (MOFs) and the reduction of PFAS by the hydrated electron (e_{aq}^-) are investigated.

A series of MOFs were synthesized using Zr(IV) salts and various neutral and cationic ligands for the adsorption of anionic contaminants in water. It was found that even though these Zr-MOFs are effective at the removal of the anionic dye Eosin Y and the environmental contaminant perfluorooctanesulfonate (PFOS) it comes at a relatively high cost. That is due to the mechanism by which the contaminant removal occurs. The data presented indicate that anionic contaminants are removed from water via an exchange mechanism where ligands comprising the struts of the MOF backbone are lost to the bulk solvent and replaced by the coordination of the contaminant at the metal-node of the MOF.

To understand the mechanism of action of e_{aq}^-, that could potentially form upon irradiation of photoactive MOFs with UV-excitation, on PFAS we have used $Fe(CN)_6^{4-}$ as a model aprotic electron donor. Herein, the benefit of using aprotic electron donors is demonstrated by comparison with the commonly used SO_3^{2-} which readily forms a Brönsted acid at pH below 10. The initial reduction reaction between the e_{aq}^- and a series of linear perfluoroalkylcarboxylates (PFxA, x = the number of carbons comprising the PFAS hydrophobic backbone) and perfluoroalkylsulfonates (PFxS) are also investigated as a baseline for future experiments using MOFs as photocatalysts for PFAS degradation. It was found that the initial reduction of both PFxA and PFxS by e_{aq}^- occurs with a rate constant of approximately $1x10^9$ M^{-1} s^{-1} and is independent of the PFAS chain length. Likewise, the energy of activation corresponding to the reduction of PFxA and PFxS is independent of the chain length and its magnitude (~11 kJ mol^{-1}) is indicative of a diffusion-controlled reduction reaction suggesting that reductive chemistries involving bond-breaking occur downstream of the initial reduction reaction.

This report presents research conducted by William A. Maza, Ph.D.

This page intentionally left blank.

METAL-ORGANIC FRAMEWORKS AS SORBENTS OF PERFLUOROALKYL SUBSTANCES AND THEIR REDUCTION BY THE HYDRATED ELECTRON

1. INTRODUCTION

1.1 Motivation

Per- and poly-fluoroalkane surfactants (PFAS) are a persistent and recalcitrant class of molecules. Their physical properties, particularly the high density of very stable C-F bonds (e.g. C-F bond energy ~ 127 kcal/mol, 5.5 eV for C_2F_6)[1] throughout their backbone, tend to make them resilient to metabolic and chemical degradation. Data suggest that continued exposure to PFAS may result in significant health risks.[2, 3] In 2021, the EPA announced that it would begin the process of formally designating perfluorooctanoic acid (PF8A) and perfluorooctane sulfonic acid (PF8S) as hazardous substances. A report published in 2020 by the Nordic Council of Ministers estimates that PFAS pollutant exposure has led to anywhere between 600 to 700 deaths in Nordic countries alone carrying a health cost of up to ~$2.7 billion.[4] In the same report healthcare costs and environmental damages arising from exposure to PFAS contaminants were estimated to be $52-84 billion and $16.9 billion, respectively, in the EU; similar estimates were given for the US (i.e. $37-59 billion in healthcare costs and $12.1 billion in environmental damages). As a result, the increasing environmental footprint of PFAS has generated alarm among regulators, government officials and, more recently, the general public.[5] Decontamination efforts aimed at removing PFAS from the environment have proven challenging due to their amphoteric nature and, more importantly, exceptional stability that results in their environmental persistence.[6] There is, therefore, a continued interest in developing novel materials and technologies designed to remove and degrade PFASs from contaminated ground soil and waters while also being easily regenerated.

1.2 Current State-of-the-Art: Sorbents of PFAS

The current state-of-the-art of PFAS removal from ground soil and water involves filtration through activated carbon (AC) or ion exchange resins (IER). These each have their limitations, however. For example, Ross, *et al*.[7] summarized that 1) AC demonstrates good retention of longer chain PFASs but performs more poorly with shorter chain variants, 2) IERs tend to do better over a range of PFAS chain lengths generally showing comparatively poorer performance with longer PFASs than with shorter variants, and that 3) both AC and IER display little activity to C1 and C2 PFASs. Because of these drawbacks, new materials are needed which can immobilize all PFAS derivatives regardless of chain length.

Open porous frameworks, like metal-organic frameworks (MOFs), have already demonstrated promise as scaffolds for chemoselective filtration.[8-11] MOFs are comprised of repeating organic units bridged by coordinating metal nodes. The porosity and morphology of the frameworks are easily tunable by modification of the organic unit size and symmetry, or choice of metal at the connecting nodes.[12-14]

To date, only a few examples of MOFs have been explored for the sorption of PFASs.[15-18] These reports employed water-stable MOFs such as those comprised of Zr(IV) metal-oxo nodes. In particular, Li et al.[19] focused on UiO-66 in which the organic ligand is terephthalic acid and NU-1000 whose ligand is 1,3,6,8-tetrakis(p-benzoic acid)pyrene. In that report, the authors found that of the twenty-eight PFASs studied UiO-66 and NU-1000 displayed a general preference for sorption of long chain PFAS, performing comparatively poorer at adsorption of short chain PFAS.

Manuscript approved February 7, 2022.

1.3 Current State-of-the-Art: Degradation of PFAS

Advanced reduction methodologies involving the degradation of PFASs in water by the generation of high energy hydrated electrons (e_{aq}^-) have garnered considerable attention.[20, 21] The e_{aq}^- has been demonstrated to effectively reduce both perfluoroalkyl carboxylates (PFxAs, x = number of carbons comprising the surfactant hydrophobic tail) and perfluoroalkyl sulfonates (PFxSs).[22-31] PFxSs are more resistant to highly oxidative conditions than are PFxAs and, therefore, are more difficult to treat by conventional methods.[32] In contrast, reductive processes involving UV-exposure of solutions containing Na_2SO_3 or KI to produce e_{aq}^- have shown considerable success in the degradation of both perfluorooctanoate (PF8A) and perfluorooctane sulfonate (PF8S, Scheme 1).[23, 24, 27, 30, 33, 34] The degradation reaction is mediated by the formation of e_{aq}^- from SO_3^{2-} or I^- upon UV-irradiation by photodetachment with subsequent reduction of the PFAS.[23, 24, 29, 34-36]

UV-irradiation of solutions containing SO_3^{2-} under basic conditions (pH > 8) effectively degrades PFAS as a result of the reaction with hydrated electrons, e_{aq}^-.[23, 24, 35] These hydrated electrons are generated by UV photodetachment of aqueous SO_3^{2-} anions. The large standard reduction potential (- 2.9 V)[37] of the e_{aq}^- is energetically analogous to the potentiometric biases required for the defluorination reaction of many perfluoroalkanes (e.g. $E°_{PFOA} \sim 2.5$ V vs SHE and $E°_{PFOS} < 3.2$ V vs. SHE estimated based on the biases required for decomposition at the cathodes of the electrochemical cells employed).[26, 38-41] However, the use of SO_3^{2-} as a source of e_{aq}^- has a significant drawback because of its decreased degradation efficiency with decreasing pH.

PFOS degradation by UV-irradiated SO_3^{2-} is most effective at pH values > 8 and is negligible at pH < 7.[24] We recently reported that the cause of this pH range limitation is the quenching of e_{aq}^- by sulfite's conjugate acid, HSO_3^-,present at intermediate pH values.[42] Therefore, alternative photochemistries that support e_{aq}^- survivability at lower pH are of interest.

2. APPROACH

2.1 MOFs as sorbents of PFAS

In this report, we expanded on the work of Li, et al.[19, 43] using UiO-66 as a PFAS sorbent believing the sorption capacity of the MOF could be improved for anionic contaminants, like PF8S and PF8A, by modifying the terephthalic acid (new ligand **1**) to include cationic moieties (Scheme 2), thereby leveraging Coulombic interactions with the anionic contaminants. We also synthesized a viologen derivative **2** (Scheme 3) as an attempt to further increase the positive charge density of the MOF. Before testing the MOFs affinity for PFAS, they were screened using the anionic dye Eosin Y (Scheme 1).

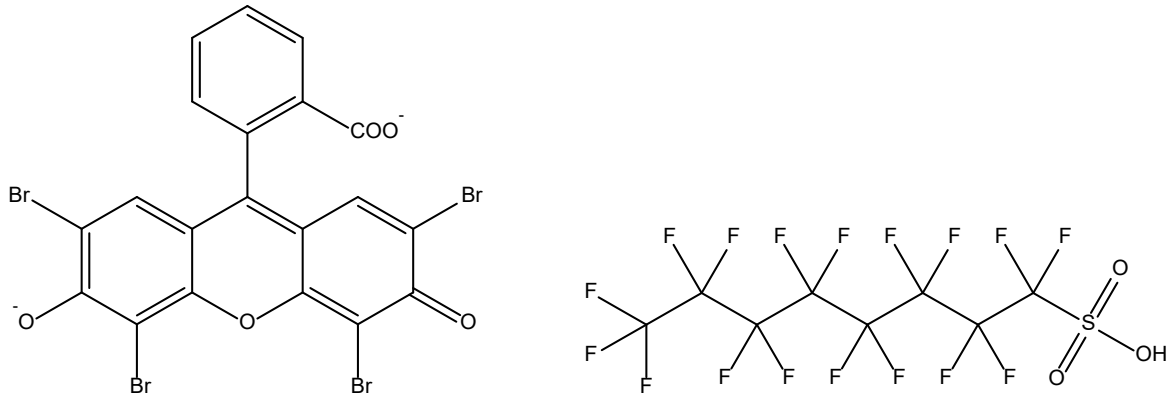

Scheme 1. Chemical structures of (left) Eosin Y (EY) and (right) perfluorooctanesulfonic acid (PFOS).

2.2 Aprotic materials as sources of e_{aq}^-

To understand the potential mechanism of action of e_{aq}^- formed from photoactive open-framework materials, like MOFs or COFs, we have expanded on previous investigations using nanosecond transient absorption spectroscopy to parse the effect of weak Brönsted acids, like HSO_3^-, on the lifetime of the e_{aq}^- by examining the dependence of the e_{aq}^- lifetime on pH in the absence of weak acids in solutions of $K_4Fe(CN)_6$.[42] The quenching of e_{aq}^- by PFAS is monitored by nanosecond transient absorption spectroscopy in solutions of Na_2SO_3 and $K_4Fe(CN)_6$. This is meant to probe the kinetics of the first reduction step in the PFAS degradation reaction by e_{aq}^-, which we show are similar between solutions of Na_2SO_3 and $K_4Fe(CN)_6$. Specifically, we show that the observed rate constant corresponding to the e_{aq}^- scavenging by PFAS is independent of pH in solutions of Na_2SO_3 and $K_4Fe(CN)_6$.

Ferrocyanide is a well-studied precursor for generating solvated electrons via photodetachment and, for several reasons, is a particularly attractive alternative to SO_3^{2-} to model the behavior of e_{aq}^- quenching by PFOS in the absence of Brönsted acids. Unlike SO_3^{2-} ($pK_b = 6.8$), $Fe(CN)_6^{4-}$ is both aprotic at pH > 4.3 and has a larger molar extinction coefficient (ε) at excitation wavelengths < 300 nm (SO_3^{2-} $\varepsilon_{254nm} \sim 50\ M^{-1}\ cm^{-1}$; $Fe(CN)_6^{4-}$ $\varepsilon_{254nm} \sim 5000\ M^{-1}\ cm^{-1}$).[42, 44-47] Ferrocyanide also has a high quantum yield of photodetachment even in the near UV;[48] the quantum yield of e_{aq}^- detachment (Φ_e) from $Fe(CN)_6^{4-}$ approaches unity with increasing incident photon energy (SO_3^{2-} $\Phi_e \sim 0.1$ at 254 nm excitation, pH 8; $Fe(CN)_6^{4-}$ $\Phi_e \sim 0.65$ at 254 nm excitation, pH 8).[47]

Besides SO_3^{2-} and $Fe(CN)_6^{4-}$, other photochemically active anions capable of producing e_{aq}^- are also known. Examples include iodide (I^-) solutions which, in the absence [27, 28, 33] and presence of [36] SO_3^{2-}, produce e_{aq}^-. However, in comparison, the quantum yield of e_{aq}^- detachment for both SO_3^{2-} and I^- is considerably lower than that of $Fe(CN)_6^{4-}$ at all excitation wavelengths.[47] In addition, the degradation of PFOS in solutions of both SO_3^{2-} and I^- are sensitive to weak conjugate acids that form at pH < 8. $Fe(CN)_6^{4-}$, on the other hand, has a pK_a between 4.1 and 4.4.[49, 50] It will be demonstrated here that quenching of e_{aq}^- in solutions of $Fe(CN)_6^{4-}$ is negligible at pH > 5.

2.3 Reduction of PFAS by the e_{aq}^-

An understanding of the e_{aq}^- mediated mechanism of degradation governing PFAS decomposition has yet to be fully elucidated. Recent reports on first principles theoretical studies have attempted to advance our understanding of the elementary steps of the reaction pathway.[30, 40, 51] For example, in a report combining both experimental and theoretical results Bentel, et al.[30] demonstrated a strong dependence of the rate of degradation and defluorination of PFxS on the carbon chain length. However, the bond dissociation energies (BDE) calculated by DFT, in the same report by Bentel,[30] could not explicitly explain this difference. In particular, they were unable to explain the lack of a chain length dependence on the experimental rate constants corresponding to the degradation of PFxA despite the bond dissociation energies for the most vulnerable CF_2 units in PFxS and PFxA being similar in magnitude (~ 447 kJ mol^{-1}). van Hoomisen and Vyas[40] recently reported on the vertical binding energies (VBE) and adiabatic electron affinities (AEA) for a number of PFxA and PFxS of varying chain length between three and eight perfluorinated carbons. Although the BDE, VBE, and AEA can be used to estimate the free energy associated with the reduction of PFAS and, therefore, the rate of reduction, they cannot fully predict the probability of reaction as other factors must also be taken into consideration. Their results, however, suggest that there should be no chain length dependence on the initial reduction of PFxA and PFxS, which contradicts experimental results found in the literature.[30, 33] As of now, there is little experimental data describing the initial reactions in the degradative pathway involving e_{aq}^- and PFAS.

To date, the only report with a kinetic analysis of the reaction between e_{aq}^- and PFxA performed on the microsecond timescale found nearly an order of magnitude difference in the rate constant for the initial reduction of PF8A and PF2A by e_{aq}^-.[52] This chain length dependence contradicts what has been both theoretically proposed,[40] as well as found experimentally for long-term degradation of PFxA.[30, 33] Here we revisit this question using nanosecond transient absorption spectroscopy for PFxAs, and PFxSs of varying carbon chain lengths. It is important to stress that the processes described herein, which occur on the

microsecond timescale, should not be conflated with complete degradation of PFxA or PFxS, since that is more complex and involves a number of redox, elimination, and rearrangement reactions. The data presented in this report comprise only the first step(s) of the overall degradation, but is nonetheless significant and indispensable in understanding the degradation process as a whole.

3. EXPERIMENTS

3.1 Synthesis of Zr-MOFs

*3.1.1 Synthesis of N-(2',4'-Dinitrophenyl)pyridinium chloride, **2***

The precursor compound **2** was synthesized similar to what has been previously reported.[53] A 20 mL high pressure flask was charged with 4 mL pyridine (49 mmol) and 10 g 1-chloro-2,4-dinitrobenze (49 mmol). The solution was then heated to 95 °C with stirring for > 1hr. This produced an off-white color solid that was washed with acetone, filtered, washed further with acetone, and dried in a convection oven at 70 °C for two days. The ^{1}H NMR spectrum is shown in Figure 1a.

3.1.2 Synthesis of 2-pyridiniumbenzene-1,4-dicarboxylic acid, BDC-pyr$^+$

2-Aminobenzene-1,4-dicarboxylic acid (BDC-NH_2, 1.5 g, 8.3 mmol) and **2** (4.75 g, 16.5 mmol) were placed in a 200 mL high pressure flask containing 80 mL EtOH. The flask was sealed and the solution was heated at 100 °C for 3 days. After cooling the solution to room temperature the solution was added to THF producing a yellowish solid which was filtered and washed with THF and acetone. The ^{1}H NMR spectrum is shown in Figure 1b.

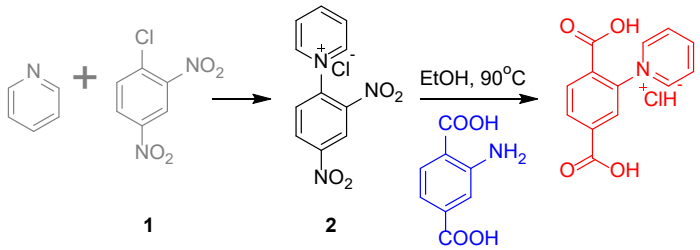

Scheme 2. Synthesis of 2-pyridiniumbenzene-1,4-dicarboxylic acid (BDC-pyr$^+$).

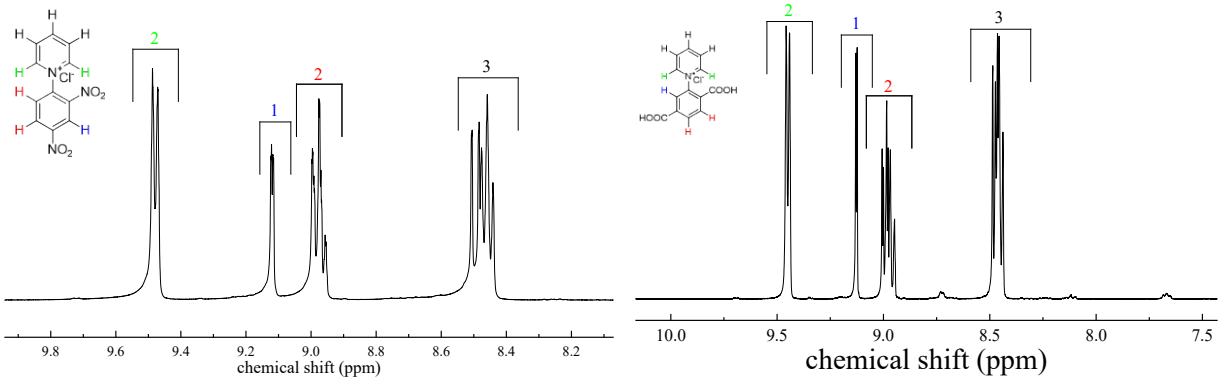

Figure 1. ^{1}H NMR of compound **2** (left panel) and BDC-pyr$^+$ (right panel).

3.1.3 Synthesis of UiO-66

The general synthesis of UiO-66 (Figure 2) and the derivatives explored herein were as follows: a scintillation vial was charged with 0.44 mmol $ZrCl_4$ and 0.44 mmol benzene-1,4-dicarboxylic acid (BDC), or its derivatives 2-aminobenzene-1,4-dicarboxylic acid (BDC-NH_2) and 2-pyridiniumbenzene-1,4-dicarboxylic acid (BDC-pyr$^+$), Figure 3. Then, 10 mL dimethylformamide (DMF) and 1mL glacial acetic acid were added. The scintillation vial was then sealed and heated in a convection oven at 120 °C. After

twelve hours of heating the vials were then allowed to cool to room temperature, filtered, the solid washed with fresh DMF (~50 mL x2) and acetone (~50 mL), and allowed to dry in air. X-ray powder diffraction patterns are shown in Figure 3.

Attempts of synthesizing a variant of UiO-66 using BDC-pyr$^+$ as the only ligand were fruitless; there was either no product formed or an amorphous solid resulted. Therefore, the procedure was modified so that the synthesized Zr-MOF contained both BDC and BDC-pyr$^+$ in a 70% to 30% ratio, respectively. This resulted in a crystalline product of slight yellowish hue. The presence of BDC-pyr$^+$ was confirmed by diffuse reflectance spectroscopy (Figure 4).

3.1.4 Synthesis of N,N'-(2,4-dinitrophenyl)bipyridinium dichloride, ***3***

A high pressure flask was charged with 6.2 g (36 mmol) 4,4'-bipyridine, 17 g (84 mmol) 1-chloro-2,4-dinitrobenzene, and 70 mL EtOH. The flask was sealed and the solution heated to 90 °C with stirring for 24 hrs upon which a brown precipitate formed. After cooling to room temperature, the precipitate was filtered and the solid extensively washed with EtOH and dried in air. The ^{1}H NMR spectrum is shown in Figure 5.

3.1.5 Synthesis of N,N'-(4-benzoic acid)bipyridinium dichloride, BPY-BZA$_2$Cl$_2$

Synthesis of BPY-BZA$_2$Cl$_2$ was carried out using a modified procedure to what was reported by Sui, et al.[54] A high pressure flask was charged with 2.7 g (5.2 mmol) **3**, 3.4 g (25 mmol) 4-aminobenzoic acid, and 80 mL EtOH. The solution was heated to 100 °C with stirring for 48 hrs. After cooling to room temperature, the precipitate was filtered and washed extensively with EtOH and later air dried. The ^{1}H NMR spectrum is shown in Figure 5.

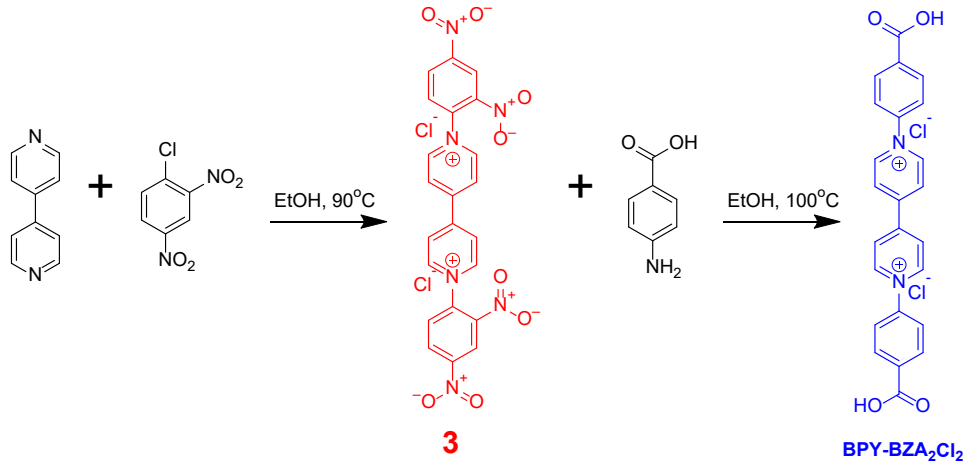

Scheme 3. Synthesis of N,N'-(4-benzoic acid)-bipyridinium (BPY-BZA$_2^{2+}$).

3.1.6 Synthesis of catZrMOF-1

A scintillation vial was charged with 200 mg (0.6 mmol) $ZrOCl_2 \cdot 8H_2O$, 188 mg BPY-BZA$_2$Cl$_2$, 15 mL DMF, and 5 mL formic acid. The solution was heated under autogenous pressure at 120 °C for 72 hrs. After cooling to room temperature, the solid product was filtered and washed with DMF and acetone. X-ray powder diffraction pattern of the product obtained is similar to that of the PIZOF-1 MOF (Figure 6) previously reported and is shown in Figure 7.

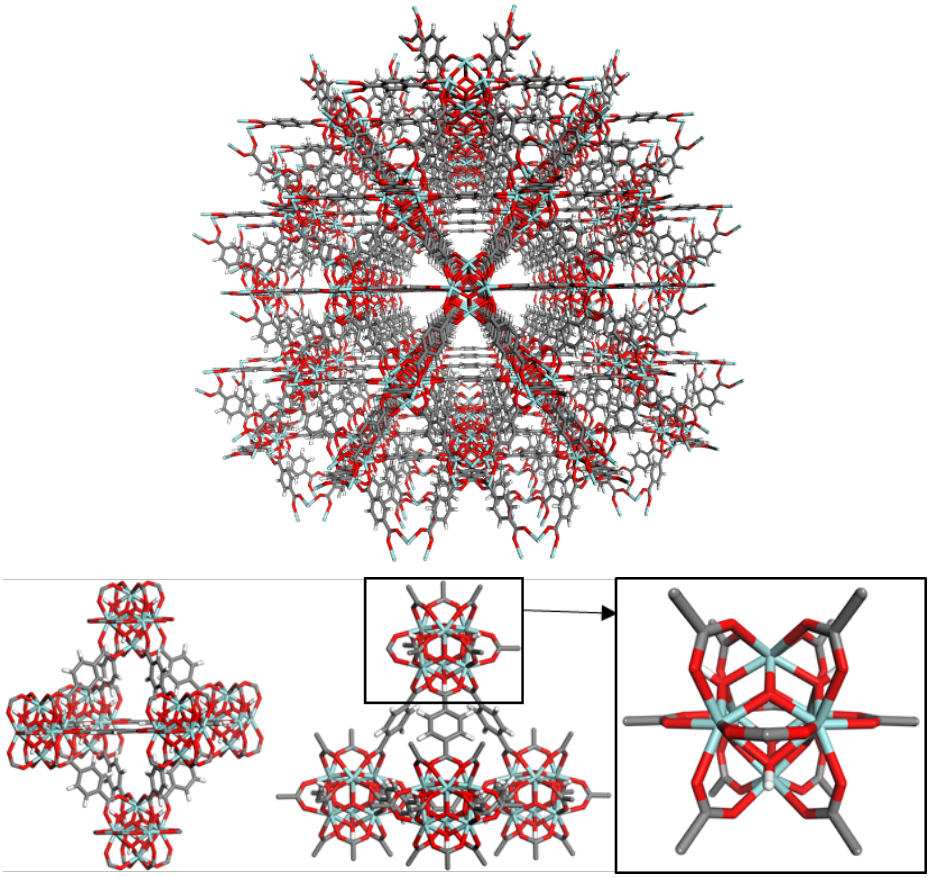

Figure 2. (Top) Depiction of the crystallographic structure of the UiO-66 MOF (adapted from structural information obtained from reference [55], CCDC structure ID 889529). (Bottom) A close-up view of the octahedral (left) and tetrahedral (middle) cavities, as well as the $Zr_6(\mu\text{-}O)_4(OH)_4(COO)_{12}$ metal-oxo nodes of the MOF.

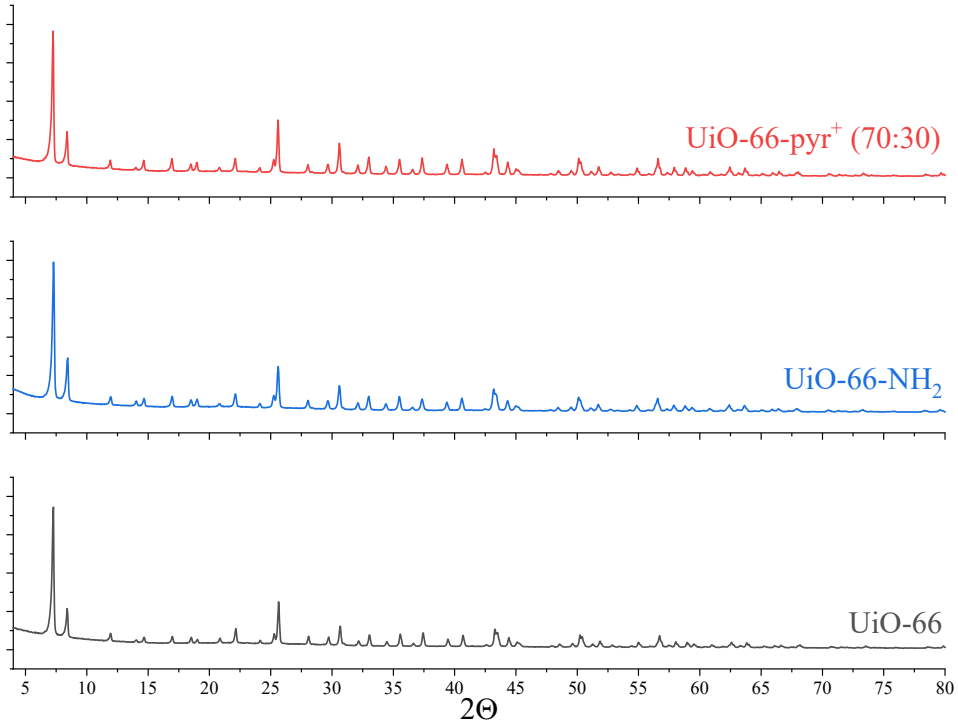

Figure 3. Powder X-ray diffraction patterns of as synthesized UiO-66 (black), UiO-66-NH2 (blue), and UiO-66-pyr$^+$ (70:30, red).

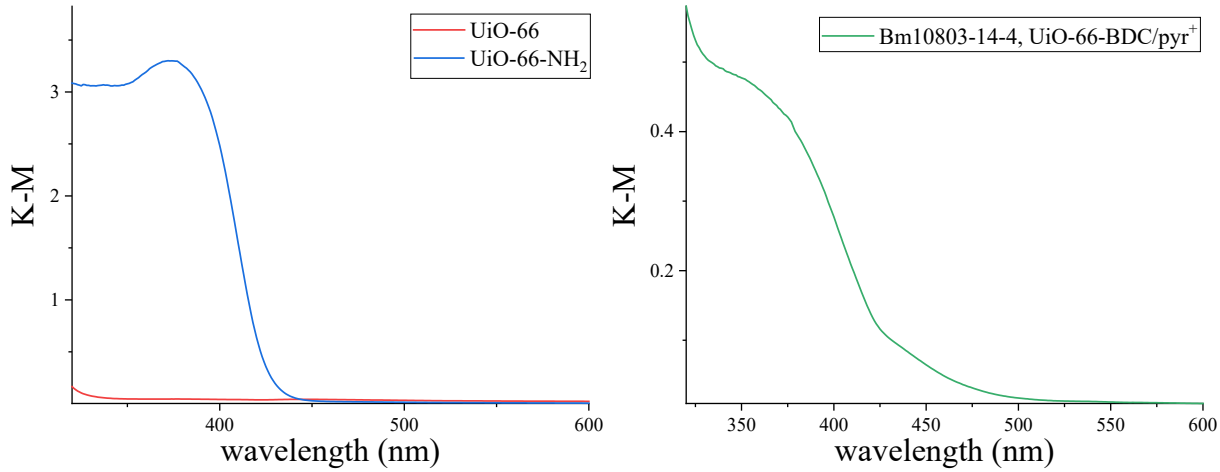

Figure 4. Diffuse reflectance spectra of (left panel) UiO-66 (red), UiO-66-NH$_2$ (blue), and (right panel) UiO-66-pyr$^+$ (green).

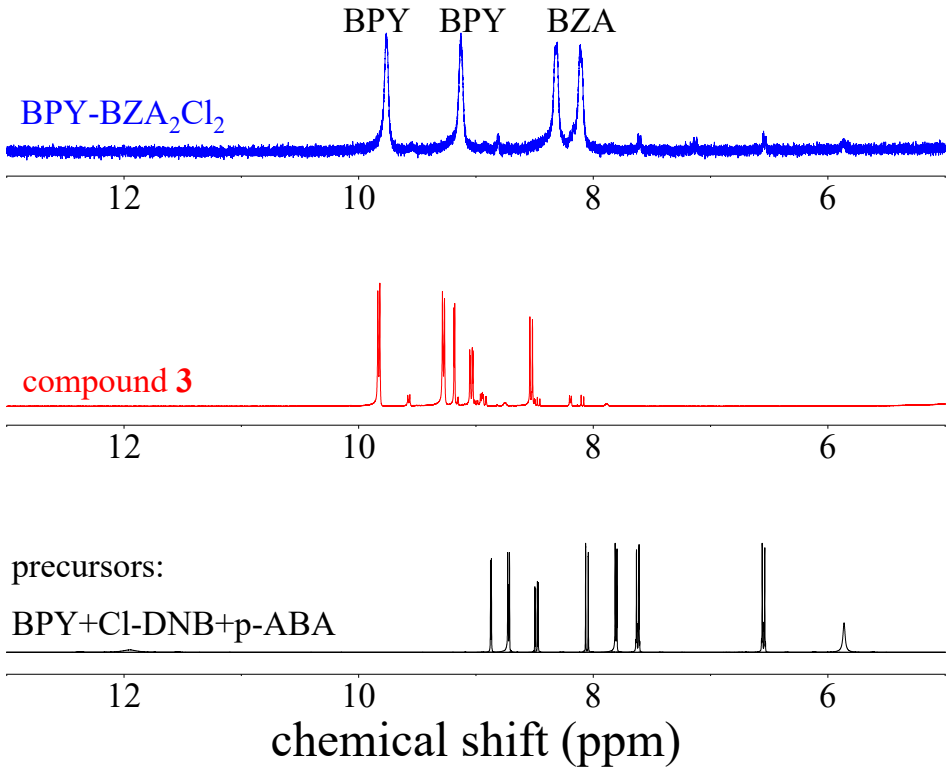

Figure 5. ^{1}H NMR of 4,4'-bipyridine and 1-chloro-2,4-dinitrobenzene precursors (black), compound **3** in dmso (red), and BPY-BZA$_2$Cl$_2$ in D$_2$O (blue).

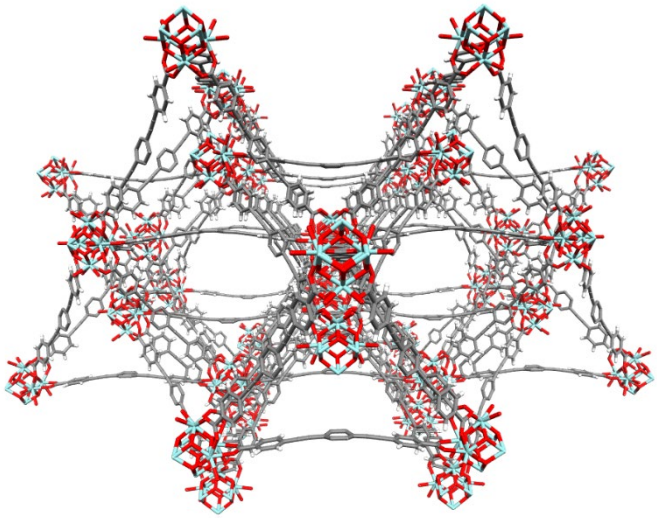

Figure 6. Depiction of the crystallographic structure of the PIZOF-1 MOF (adapted from structural information obtained from reference[56], CCDC structure ID 803459).

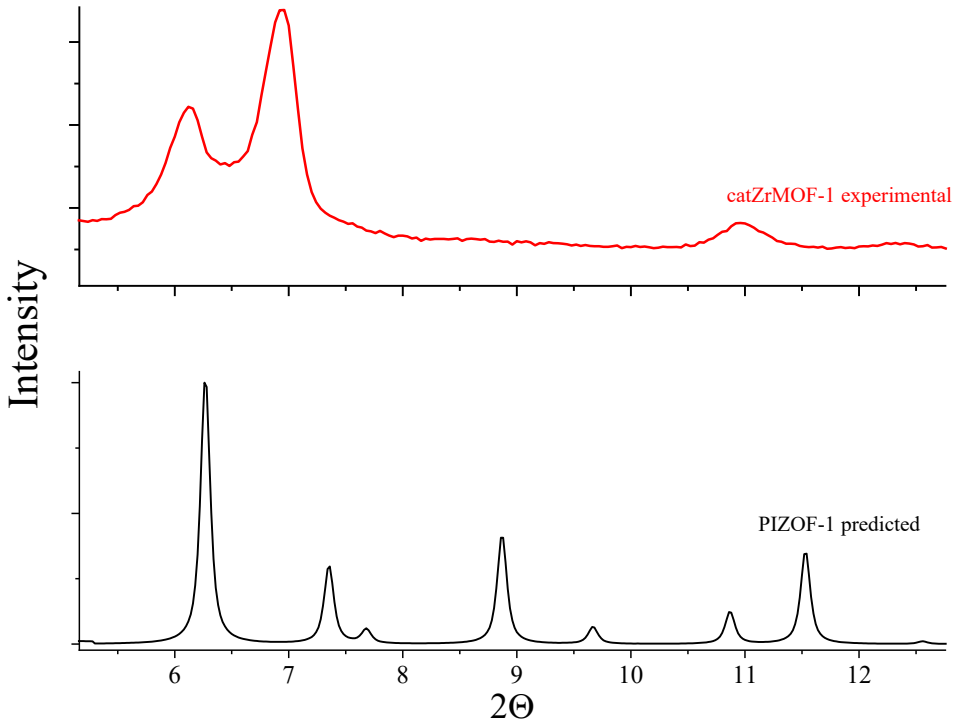

Figure 7. Powder X-ray diffraction pattern of catZrMOF-1 (red) and the predicted powder pattern of PIZOF-1 (black, from CCDC structure ID 803459).

3.2 Determination of the removal of the anionic dye Eosin Y from water

The determination of Eosin Y (EY) uptake by the MOFs described above was done by preparing a 2 μM solution of EY in 100 mL of deionized water. To this solution 10 mg MOF was added and the solution stirred over the course of 30 min. The UV-visible absorbance was monitored over the course of the 30 min to determine the amount of dye remaining in solution.

3.3 Determination of PFAS adsorption capacity

The catZrMOF-1 was evaluated for PFAS adsorption by suspending a given mass of MOF in 100 mL of a 100 μM aqueous solution of PFOS. Aliquots were periodically removed and filtered using 0.1 μm polypropylene syringe filters for quantitative analysis by LC-MS.

3.4 Nanosecond Transient Absorption.

Stock solutions of Na_2SO_3 and $K_4Fe(CN)_6$ were prepared fresh before each analysis. Samples used for transient absorption experiments were prepared in a standard 1 cm pathlength quartz cuvette from a freshly prepared stock solution. The final concentrations were 10 mM Na_2SO_3 and 40 μM $K_4Fe(CN)_6$ in deionized water. The samples were de-aerated and dissolved O_2 removed by bubbling with N_2. Stock solutions of PFOS were prepared at the solubility limit of 1 mM (pH ~ 7). The pH of the sample solution was adjusted using either $HClO_4$ or NaOH before addition of PFOS.

The geometry of the home-built transient absorption instrumentation used has been described previously.[42] Samples were irradiated with the fourth harmonic output of a Continuum Minilite II Nd:YAG laser (266 nm, 5 ns pulse width, 200 μJ/pulse). The lifetime of the e_{aq}^- generated from the 266 nm irradiation was probed using a 790 nm continuous wave diode laser (Thorlabs model CPS780S). Both the 266 nm pump and 790 nm probe were directed into the sample co-linearly. The change in intensity of the

790 nm probe was monitored using a Hamamatsu R375 photomultiplier tube (9 ns rise time, 70 ns transit time) and digitized on a Tektronix TDS 420A oscilloscope (200 MHz, 100 MS s–1 sampling rate) triggered by the firing of the laser Q-switch. Each transient shown represents the average of at least 300 shots. Sample solutions were stirred during the acquisition of the e_{aq}^- lifetimes.

4. RESULTS AND DISCUSSION

4.1 Removal of Eosin Y from water

The anionic dye Eosin Y (EY) is a small water-soluble dye displaying strong absorbance in the visible spectrum with a molar extinction coefficient of 54.6 mM^{-1} cm^{-1} at 517 nm making it easy to track its removal from aqueous solutions using UV-visible absorbance spectroscopy (Figure 8). Incubation of 10 mg UiO-66 with 2 µM EY resulted in a nearly 48 % removal of EY after 30 min. Similarly, a 46 % removal of EY was observed after 30 min when incubated with UiO-NH_2. However, the adsorption kinetics were found to be quite distinct despite the similarity in the total removal of EY between UiO-66 and UiO-66-NH_2. Specifically, UiO-66-NH_2 displayed faster adsorption kinetics compared to UiO-66 with rates of adsorption of 0.15 min^{-1} and 0.06 min^{-1}, respectively. Alternatively, UiO-66-BDC-pyr^+ displayed both slightly lower EY adsorption capacity, removing only 41 % of EY, and slightly slower adsorption kinetics, rate of adsorption of 0.05 min^{-1}, compared to UiO-66 and UiO-66-NH_2. The reason for this is not readily apparent, but may be a result of restricted access to, and/or occlusion of, the pores by the pyridinium groups.

We expected to improve on the performance of UiO-66-BDC-pyr^+ by extending the cationic ligand size and, therefore, the porosity of the Zr-MOF, as well as increasing the charge of the ligand. Based on the dimensions of the ligand and the resulting PXRD powder pattern of the synthesized catZrMOF-1, it is expected to have similar topology and porosity as the reported PIZOF-1 (surface area ~ 2020 m^2 g^{-1}, pore size ~ 19 Å).[56] Indeed, catZrMOF-1 demonstrated higher adsorption capacity (~ 57 %) compared to the UiO-MOFs, and rate of adsorption of 0.22 min^{-1}.

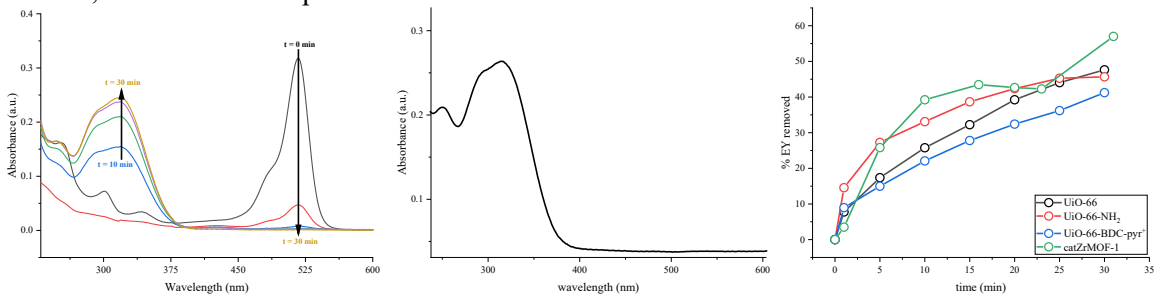

Figure 8. (Left panel) UV-visible absorption spectrum of a 2 µM aqueous solution of EY in the absence (black line) and presence (red, blue, green, purple, and orange lines) of 10 mg catZrMOF-1 taken over the course of 30 min. (Middle Panel) UV-visible absorbance spectrum of a 10 µM aqueous solution of BPY-BZA_2Cl_2. (Right panel) Fractional removal kinetics of EY from water for UiO-66 (black), UiO-66-NH_2 (red), UiO-66-BDC-pyr^+ (blue), and catZrMOF-1 (green).

For all MOFs, the decrease in the EY absorbance observed as a function of time was accompanied by an increase in absorbance in the UV and near-UV regions of the spectrum. This increase in absorbance is attributed to the concomitant release of MOF ligands into solution with EY adsorption. This is best observed in the catZrMOF-1 case (Figure 8) in which the loss of the EY absorbance band at 517 nm is accompanied by the emergence of a new band having a maximum at 319 nm and a shoulder 294 nm. These electronic transitions are characteristic of the BPY-BZA_2Cl_2 absorbance in water (Figure 8). We, therefore, propose a mechanism of EY adsorption that involves displacement of a MOF ligand at coordinative-sites of the MOF metal-nodes and replacement by the dye (Scheme 4). This is supported by comparing the rate of the emergence of the absorbance corresponding to BPY-BZA_2^{2+} at 319 nm (0.219 min^{-1}) to the loss of the absorbance corresponding to EY at 517 nm (0.217 min^{-1}).

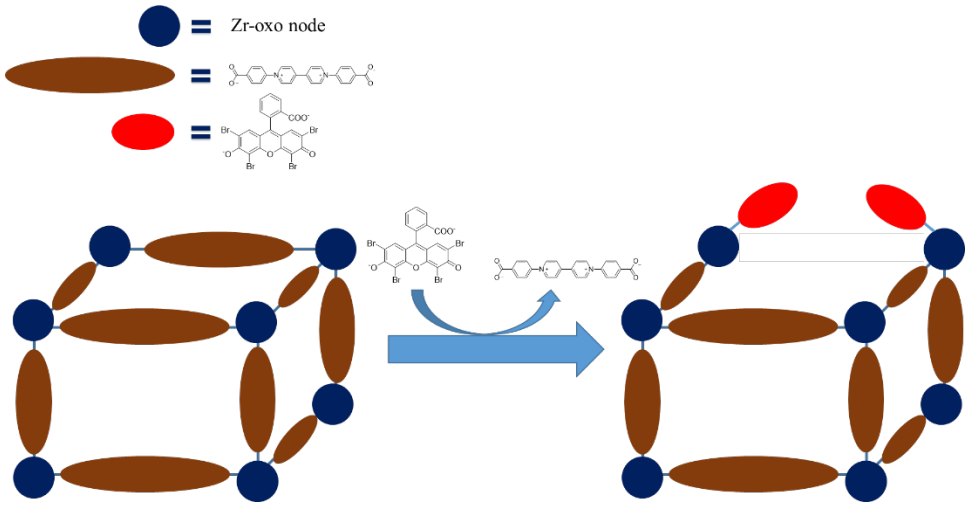

Scheme 4. Proposed mechanism of dye adsorption by catZrMOF-1. The same general scheme is proposed for the UiO-MOFs probed here also.

4.2 Removal of PFOS from water

Based on the results of the contaminant removal experiments using EY with the various MOFs probed, the capacity of catZrMOF-1 for PFOS adsorption was examined. Suspending > 10 mg catZrMOF-1 was sufficient to observed some adsorption of PFOS in solutions containing 100 µM PFOS. At 10 mg catZrMOF-1 a ~ 17 % removal of PFOS was observed which increased to ~ 47 % removal in the presence of 15 mg catZrMOF-1. The data indicate that catZrMOF-1 has an adsorption capacity of 0.47 mol kg^{-1} for PFOS which is somewhat larger than what has been reported for commercial granulated activated carbon (GAC), ~ 0.37 mol kg^{-1}. The adsorption capacity found here is nearly three times smaller than the 1.24 mol kg^{-1} that was found for the NU-1000 by Li, et al.;[43] however, their reported value is likely inflated as the authors used nylon filters, known to have high affinity for PFOA and PFOS,[57] prior to LCMS analysis.

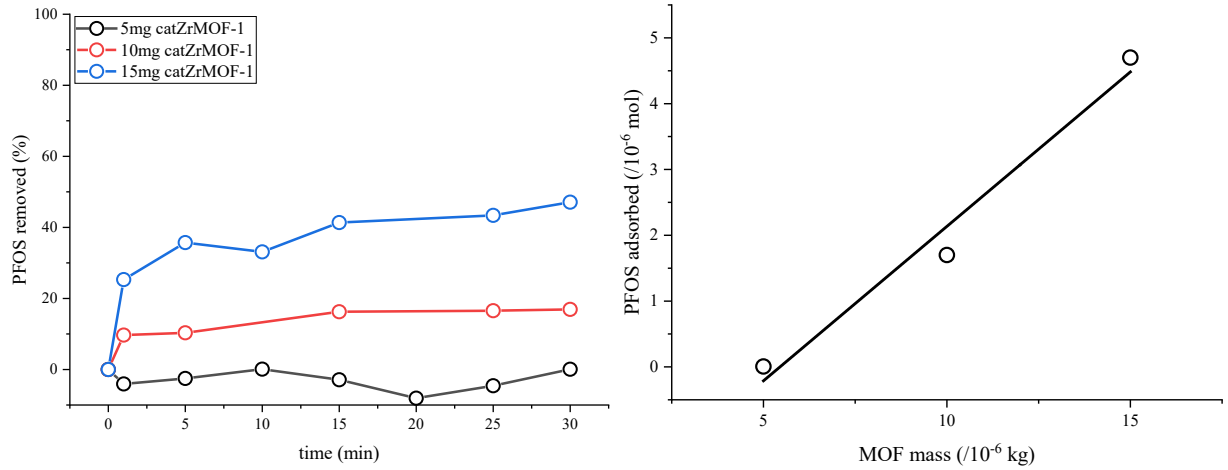

Figure 9. (Left panel) Adsorption kinetics of PFOS on varying amounts of catZrMOF-1. (Right panel) Adsorption isotherm of PFOS on catZrMOF-1 for the determination of PFOS adsorption capacity of the MOF.

4.3 Na_2SO_3 vs. $K_4Fe(CN)_6$: pH effect on e_{aq}^- lifetime.

Irradiation of aqueous solutions containing either Na_2SO_3 or $K_4Fe(CN)_6$ with a 266 nm ~ 5 ns pulse produces a transient signal on the microsecond timescale at 790 nm corresponding to the near IR absorption of the photodetached e_{aq}^-.[58-60] At pH 9, the lifetimes obtained for the e_{aq}^- produced from a 10 mM solution of Na_2SO_3 or a 40 µM solution of $K_4Fe(CN)_6$ are 9.1 ± 0.2 µs and 7.4 ± 0.2 µs (Figure 1), respectively. In

both Na_2SO_3 and $K_4Fe(CN)_6$ the e_{aq}^- lifetime is sensitive to pH, although this sensitivity differs in magnitude for the two species. In Na_2SO_3, the e_{aq}^- has a lifetime that approaches 10 μs at pH > 9 (Figure 10). However, the e_{aq}^- lifetime was found to decrease sharply at pH < 9 down to a lower limit at pH ~ 5. The origin of the decrease in lifetime of the e_{aq}^- between pH 5 and 10 in Na_2SO_3 solutions has been discussed in detail[42] and is attributed to the quenching of e_{aq}^- by HSO_3^-, present in solution below pH 9 due to the SO_3^{2-}/HSO_3^- equilibrium (HSO_3^- pKa = 7.2).

The quenching of e_{aq}^- by HSO_3^- was determined from the pH dependence of the e_{aq}^- lifetime using a kinetic model which takes into account the reaction of the e_{aq}^- in water (reaction **1**)[58], non-geminate recombination between SO_3^- and e_{aq}^- (reaction **2**), reduction of SO_3^{2-} by the homogeneous quenching of e_{aq}^- (reaction **3**), and reduction of HSO_3^- by e_{aq}^- (reaction **4**).[42] The observed lifetime as a function of pH, $[SO_3^{2-}]$, $[SO_3^-]$, and $[HSO_3^-]$ can then be modelled by equation **5** below.

$$e_{aq}^- + H_2O \xrightarrow{k_{1a}} H\cdot + OH^- \quad (1a)$$

$$e_{aq}^- + e_{aq}^- \xrightarrow{k_{1b}} H_2 + 2OH^- \quad (1b)$$

$$SO_3^- + e_{aq}^- \xrightarrow{k_2} SO_3^{2-} \quad (2)$$

$$SO_3^{2-} + e_{aq}^- \xrightarrow{k_3} products \quad (3)$$

$$HSO_3^- + e_{aq}^- \xrightarrow{k_4} SO_3^{2-} + H^\bullet \quad (4)$$

$$\tau_{obs} = \left(k_{1a}[H_2O] + k_{1b}\left[e_{aq}^-\right] + k_2[SO_3^-] + k_3[SO_3^{2-}] + k_4[HSO_3^-]\right)^{-1} \quad (5)$$

This model has adequately described[42] the interaction of e_{aq}^- with HSO_3^- at pH > 5 but neglects the interaction of e_{aq}^- with H^+. Extending this model to include the reduction of H^+ according to reaction **6**, since $[H^+]$ is non-negligible at pH < 5, leads to the inclusion of an additional term to yield equation **7**.

$$H^+ + e_{aq}^- \xrightarrow{k_5} H^\bullet \quad (6)$$

$$\tau_{obs} = \left(k_{1a}[H_2O] + k_{1b}\left[e_{aq}^-\right] + k_2[SO_3^-] + k_3[SO_3^{2-}] + k_4[HSO_3^-] + k_5[H^+]\right)^{-1} \quad (7)$$

Equation **7** can be re-written in terms of the initial SO_3^{2-} concentration, $[SO_3^{2-}]_o$, the pK_a of the HSO_3^-/SO_3^{2-} equilibrium, and the solution pH to yield equation **8a**.

$$\tau_{obs} = \frac{10^{pH}+10^{pKa}}{k_4 10^{pKa}[SO_3^{2-}]_o + \frac{10^{pH}+10^{pKa}}{\tau_o} + k_5(1+10^{pKa-pH})} \quad (8a)$$

In equation **8a**, τ_o is the reciprocal of the sum of the first four terms in equation **7**

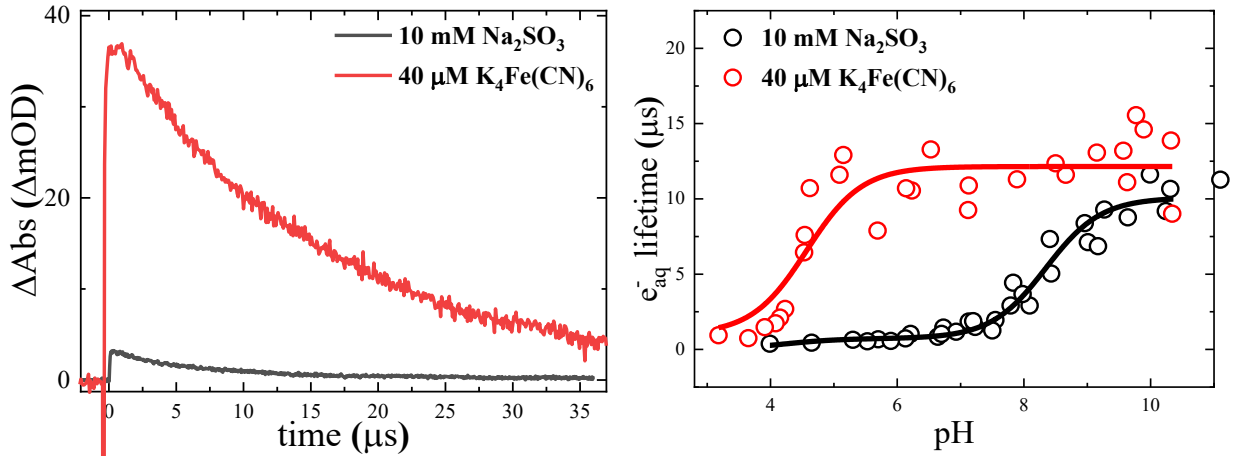

Figure 10. (Left panel) Transient absorption of the e_{aq}^- acquired at 790 nm in aqueous solutions of 10 mM Na_2SO_3 (black circles) and 40 µM $K_4Fe(CN)_6$ (red circles) at pH 9. The solid lines correspond to mono-exponential fits of the data indicative of pseudo-first order kinetics. The fitted lifetimes for Na_2SO_3 and $K_4Fe(CN)_6$ are 9.1 ± 0.2 µs and 7.4 ± 0.2 µs, respectively. (Right panel) Lifetime of the photodetached e_{aq}^- as a function of pH in solutions of 10 mM Na_2SO_3 (open black circles) and 40 µM $K_4Fe(CN)_6$ (open red circles). Solid lines represent best fits of the data to equations **8a** and **9**, respectively.

$$\tau_o = \left(k_{1a}[H_2O] + k_{1b}[e_{aq}^-] + k_2[SO_3^-] + k_3[SO_3^{2-}]\right)^{-1} \quad 8b$$

and corresponds to the e_{aq}^- lifetime at a given concentration of SO_3^{2-} in the absence of HSO_3^- (pH > 8). When the pK_a is fixed at 7.2[45, 46], fits of the e_{aq}^- lifetimes as a function of pH in 10 mM Na_2SO_3 solutions yield a τ_o and k_4 of 10.1 ± 0.3 µs and (1.3 ± 0.2)x10^8 M^{-1} s^{-1} respectively, which are in excellent agreement with previously reported results.[42, 45] Extending the pH range down to pH 4 yields a bimolecular rate constant, k_5, of (2.3 ± 0.8)x10^{10} M^{-1} s^{-1}, corresponding to the reduction of H^+ (reaction **6**). This value for k_5 is in agreement with the accepted value of 2.3x10^{10} M^{-1} s^{-1} for reaction **6**.[61, 62] When restricting the pH range of the model to pH > 5, the k_5 term fails to converge to a physically reasonable value, indicating that above pH 5 the dominant mechanism of e_{aq}^- scavenging occurs via reaction with HSO_3^- (reaction **4**), whereas at pH < 5 the reaction with H^+ (reaction **6**) dominates.[42]

The pH dependent lifetime data obtained for solutions of $K_4Fe(CN)_6$ were fit to an analogous model assuming similar underlying mechanisms in both systems. In the case of ferrocyanide, the third and fourth terms corresponding to non-geminate recombination (reaction **2′**) and homogeneous quenching (reaction **3′**) depend on $[Fe(CN)_6^{3-}]$ and $[Fe(CN)_6^{4-}]$, respectively.

$$Fe(CN)_6^{3-} + e_{aq}^- \xrightarrow{k_2'} Fe(CN)_6^{4-} \quad 2'$$

$$Fe(CN)_6^{4-} + e_{aq}^- \xrightarrow{k_3'} products \quad 3'$$

The fifth term in equation **7** is replaced with $k_4'[Fe(CN)_5(HCN)^{3-}]$ (reaction **4′**), where the pK_a' of $Fe(CN)_5(HCN)^{3-}$ is reported to be between 4.1 and 4.4 (*vide infra*).[49, 63]

$$Fe(CN)_5(HCN)^{3-} + e_{aq}^- \xrightarrow{k_4'} Fe(CN)_6^{4-} + H^\bullet \quad 4'$$

Substitution of these terms into equation **8a** results in a new expression, **9**.

$$\tau_{obs} = \frac{10^{pH} + 10^{pK_a'}}{k_4' 10^{pK_a'}[Fe(CN)_6^{4-}]_o + \frac{10^{pH} + 10^{pK_a'}}{\tau_o} + k_5'\left(1 + 10^{pK_a' - pH}\right)} \quad 9$$

Analogous to equation **8b,** τ_o represents the e_{aq}^- lifetime at a given concentration of $Fe(CN)_6^{4-}$ and includes the same analogous terms (equation **8b′**).

$$\tau_o = \left(k_{1a}[H_2O] + k_{1b}[e_{aq}^-] + k_2'[Fe(CN)_6^{3-}] + k_3'[Fe(CN)_6^{4-}]\right)^{-1} \quad 8b'$$

Physically reasonable values for each of the parameters were only possible by fixing k_4' to zero. The result of the fit is: $pK_a' = 4.3 \pm 0.1$, $\tau_o = 7.0 \pm 0.2$ µs, and $k_5' = (9.8 \pm 0.1)\text{x}10^9$ M^{-1} s^{-1}. The value obtained here for k_5' is two times smaller compared to the k_5 value found for Na_2SO_3 and what has been previously reported for quenching of e_{aq}^- by H^+ (*vide supra*). Similarly to Na_2SO_3, at pH values below 5, protons (H^+) present in solution are expected to quench e_{aq}^-. However, as mentioned previously, below pH 5 $Fe(CN)_6^{4-}$ can exist in a protonated form, $Fe(CN)_5(HCN)^{3-}$. Therefore, it is possible that at or below pH 5, $Fe(CN)_5(HCN)^{3-}$ reacts with e_{aq}^- according to reaction **4′** and that k_5' is an apparent rate constant that includes contributions from reactions 4′ and 6.

A more complex e_{aq}^- quenching mechanism by H^+ at low pH in solutions of $Fe(CN)_6^{4-}$ is possible. From an overlay of the experimental e_{aq}^- lifetimes obtained with the calculated concentrations of several species expected to be present as a function of pH, it is evident that the decrease in the observed lifetime coincides with an increase in $[H^+]$ at lower pH. (Figure 11). At pH 4 and below, the presence of $Fe(CN)_5(HCN)^{3-}$ has a negligible effect on the e_{aq}^- lifetime according to fits of the data (Figure 10) and numerical solutions (Figure **2**) to the model given by equation **9**. Alternatively, it has been proposed that $Fe(CN)_6^{3-}$ may abstract an electron from $H^\bullet$ according to reaction **10** to regenerate $Fe(CN)_6^{4-}$; reaction **10** has a bimolecular rate constant k_6 on the order of (3 to 4)x10^9 M^{-1} s^{-1}.[64-66]

$$Fe(CN)_6^{3-} + H^\bullet \xrightarrow{k_6} Fe(CN)_6^{4-} + H^+ \qquad 10$$

It is plausible, then, that formation of the highly reactive $H^\bullet$ is fast and is subsequently rapidly oxidized by $Fe(CN)_6^{3-}$ via **10**, regenerating H^+. However, the exact mechanism resulting in the two-fold decrease of k_5' in $K_4Fe(CN)_6$ relative to Na_2SO_3 is uncertain. Nonetheless, it is evident that in solutions of $Fe(CN)_6^{4-}$ the e_{aq}^- lifetime is unaffected above pH 5. This suggests that environmentally benign sources of e_{aq}^- that do not easily form conjugate acids could be employed over a broader pH range compared to solutions containing Na_2SO_3.

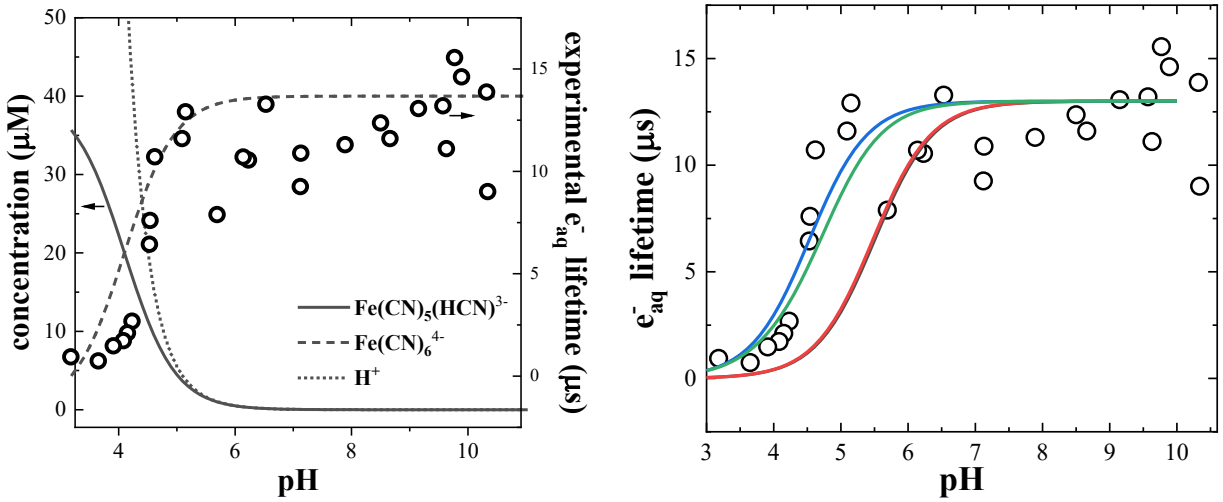

Figure 11. (Left panel) Overlay of the experimentally determined e_{aq}^- lifetimes (open circles) and predicted concentrations of $Fe(CN)_6^{4-}$ (dashed line) and $Fe(CN)_5(HCN)^{3-}$ based on the reported pK_a of 4.1 in a 40 µM solution of $K_4Fe(CN)_6$ as a function of pH. (Right panel) Overlay of the same experimentally determined e_{aq}^- lifetimes (black open circles) in a 40 µM solution of $K_4Fe(CN)_6$ as a function of pH and the predicted lifetimes (solid lines) computed using equation **9** in the main text as a function of pH by varying the magnitude of k_2 and k_3 where $[Fe(CN)_6^{4-}]_o$ was fixed at 40 µM (Black line: k2 = 3x10^9 M^{-1} s^{-1}, k3 = 2.3x10^{10} M^{-1} s^{-1}; Red line: k2 = 0, k3 = 2.3x10^{10} M^{-1} s^{-1}; Blue line: k2 = 0, k3 = 9.8x10^9 M^{-1} s^{-1}; Green line: k2 = 3x10^9 M^{-1} s^{-1}, k3 = 9.8x10^9 M^{-1} s^{-1}).

The model given by equation **9** neglects the potential role of aquapentacyanoferrate(II), $Fe(CN)_5(H_2O)^{3-}$ – which has been reported as an additional photoproduct from excitation of $Fe(CN)_6^{4-}$ at 266 nm (reaction **11**) – in the overall quenching of e_{aq}^-.[49, 67, 68]

$$Fe(CN)_6^{4-} \xrightarrow{k_7} Fe(CN)_5(H_2O)^{3-} + CN^- \qquad 11$$

It is assumed that, due to the large difference in the quantum yield of formation of the e_{aq}^- from $Fe(CN)_6^{4-}$ (Φ_e between 0.44 and 0.52 at 266 nm)[69, 70] compared to $Fe(CN)_5(H_2O)$ ($\Phi_{aquo} \sim 0.2$ at 266 nm)[67], the effect of the latter can be included in the τ_o term.

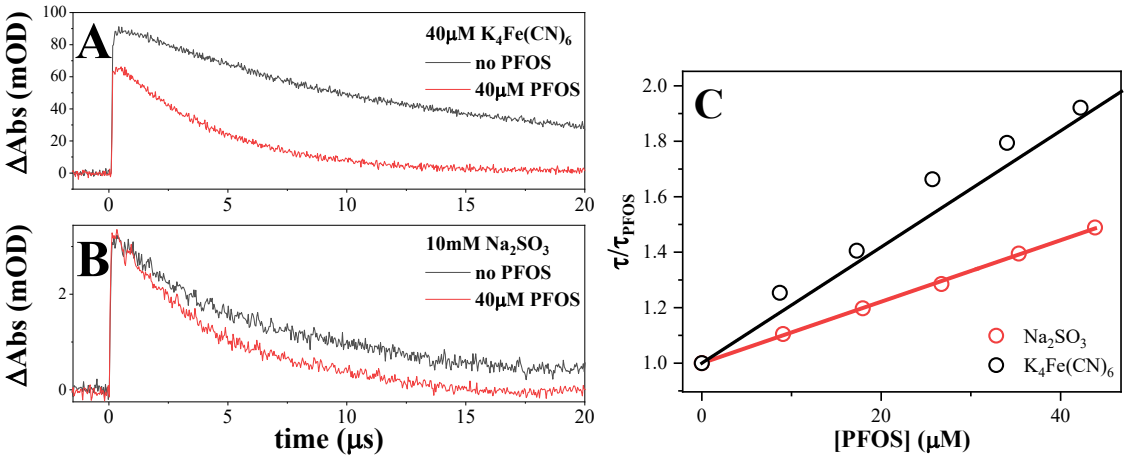

Figure 12. (Left panel, top) Transient absorption decay traces of e_{aq}^- obtained at 790 nm in a 40 μM $K_4Fe(CN)_6$ solution in the absence (black) and presence (red) of 40 μM PFOS at pH 8. (Left panel, bottom) Transient absorption decay traces of e_{aq}^- obtained at 790 nm in a 10 mM Na_2SO_3 solution in the absence (black) and presence (red) of 40 μM PFOS at pH 9. (Right panel) Stern-Volmer analysis of e_{aq}^- quenching in 10 mM Na_2SO_3 solutions at pH 9 (red open circles) and 40 μM $K_4Fe(CN)_6$ solutions at pH 8 (black open circles).

4.4 Reduction of PFOS by e_{aq}^-.

To probe the interaction of e_{aq}^- with perfluoroalkyl sulfonate, PFOS was added stepwise to 10 mM Na_2SO_3 or 40 μM $K_4Fe(CN)_6$ solutions and the transient lifetime signals were recorded. The transients obtained at 790 nm with each addition of PFOS were fit to a mono-exponential decay function. In the presence of PFOS, a decrease in the e_{aq}^- lifetime was noted in solutions of both Na_2SO_3 and $K_4Fe(CN)_6$ (Figure **3**). The bimolecular rate constants for the initial interaction of PFOS and the e_{aq}^- were determined from the decrease in the e_{aq}^- lifetime with increased [PFOS]. The observed rate constant, k_8 was obtained by a method analogous to the Stern-Volmer method (equation **12**, Figure 12):

$$\frac{\tau}{\tau_{PFOS}} = 1 + k_8\tau\,[PFOS\,] \qquad 12$$

where τ is the e_{aq}^- lifetime at any given pH in the absence of PFOS and τ_{PFOS} is the lifetime of the e_{aq}^- at the same pH in the presence of PFOS. In this way, k_8 is determined independent of other e_{aq}^- scavenging processes occurring in solution (assuming the presence of PFOS does not affect the rate constants of the side reactions). A similar methodology has been used by others to obtain quenching reaction rate constants involving e_{aq}^-.[71] The reduction of PFOS by e_{aq}^- is described by reaction **13** below.

$$C_8F_{17}SO_3^- + e_{aq}^- \xrightarrow{k_8} C_8F_{17}SO_3^{2-} \rightarrow products \qquad 13$$

In a 40 μM solution of $K_4Fe(CN)_6$ at pH 10, k_8 is $(2.9 \pm 1.4)\times10^9$ M^{-1} s^{-1}, which is in close agreement with the k_8 value of $(2.7 \pm 1.0)\times10^9$ M^{-1} s^{-1} we obtain in 10 mM Na_2SO_3. The similarity of k_8 in solutions of both Na_2SO_3 and $K_4Fe(CN)_6$ solutions suggests that the initial reaction between e_{aq}^- and PFOS described by equation **13** occurs independently of SO_3^{2-}, $Fe(CN)_6^{4-}$, or their photolysis byproducts.

4.5 Chain length dependence on the reduction of PFxA and PFxS

The lifetime, τ_o, of e_{aq}^- from 266 nm (pulse energy ~ 300 μJ) excitation of a 40 μM $K_4Fe(CN)_6$ solution is 15.3 ± 0.3 μs (Figure 13A) under N_2 when stirred vigorously. This is consistent with the reported τ_o obtained for the e_{aq}^- at similar concentrations of $K_4Fe(CN)_6$.[52, 69] The addition of an electron scavenger or quencher, such as NO_3^-, reduces the e_{aq}^- lifetime (Figure 13A) and correlates to an increase in the observed e_{aq}^- decay rate as the quencher concentration increases (Figure 13B). Therefore, monitoring the changes in the e_{aq}^- lifetime provides direct insight into the rate of reduction of an e^- acceptor such as PFxA or PFxS.

The k_q for the various PFAS were obtained by a method analogous to the Stern-Volmer equation (Equation **13**):[71, 72]

$$\frac{\tau_o}{\tau} = 1 + k_q \tau_o [Q] \quad \textbf{13}$$

Here τ_o and τ are the e_{aq}^- lifetime in the absence and presence of PFAS, respectively, and k_q is the observed e_{aq}^- quenching rate constant for the corresponding quencher, Q.

The temperature dependence on the lifetime decay was obtained in the absence and presence of each PFxA or PFxS between 10 °C and 50 °C. The temperature dependent data obtained in the absence of the PFAS were used to extract the observed quenching rate constant by fitting the e_{aq}^- decay lifetime in the presence of a known concentration of PFAS to Equation **14**

$$\Delta A = \Delta A_o exp\left[-\left(\tau_o^{-1} + k_q[PFAS]\right)t\right] \quad \textbf{14}$$

where ΔA and ΔA_o are the absorbance change at time t and t = 0, respectively, and τ_o was fixed to the e_{aq}^- lifetime obtained in the absence of PFAS at the corresponding temperature. The τ_o term includes all processes germane to the natural lifetime of the e_{aq}^- in the absence of PFAS, including geminate (Equation **15**) and non-geminate (Equation **16**) recombination by $Fe(CN)_6^{3-}$ produced upon formation of the e_{aq}^-,

$$Fe(CN)_6^{4-} \xrightarrow{266nm} [Fe(CN)_6^{3-} \cdots e^-] \xrightarrow{k_{gem}} Fe(CN)_6^{4-} \quad \textbf{15}$$

$$[Fe(CN)_6^{3-} \cdots e^-] \rightarrow Fe(CN)_6^{3-} + e_{aq}^- \xrightarrow{k_{non-gem}} Fe(CN)_6^{4-} \quad \textbf{16}$$

quenching of e_{aq}^- by non-photolyzed $Fe(CN)_6^{4-}$ (Equation **17**)[42, 73]

$$Fe(CN)_6^{4-} + e_{aq}^- \rightarrow \quad \textbf{17}$$

as well as the reactions of e_{aq}^- with water (Equation 18 and 19).[58, 74]

$$e_{aq}^- + H_2O \rightarrow H\ + OH^- \quad \textbf{18}$$

$$e_{aq}^-(H_2O) + e_{aq}^-(H_2O) \rightarrow H_2 + 2OH^- \quad \textbf{19}$$

For Equations **13** and **14**, it is assumed that the rate constants for the respective processes comprising τ_o remain unaffected in the presence of PFAS and, therefore, τ_o remains constant at a given temperature throughout the course of the experiment.

Excitation of $K_4Fe(CN)_6$ at $\lambda < 300$ nm results in photodetachment and the formation of a hydrated electron, e_{aq}^-,[48, 49, 70, 75] with a quantum yield of photodetachment, Φ_e, that approaches unity with decreasing excitation λ.[47] The e_{aq}^- displays a broad absorption in water that spans the near UV to the near-IR region with an absorption maximum at ~ 720 nm.[59, 60, 76, 77] The absorbance and lifetime of the e_{aq}^- is sensitive to the presence of an electron scavenger such as NO_3^- or MV^{2+}.[78]

Upon addition of PF8S or PF8A to solutions of $K_4Fe(CN)_6$, the observed rate of e_{aq}^- decay increases (Figure 13A and 14) as a function of the concentration of the titrant. Stern-Volmer analysis of the e_{aq}^- lifetime as a function of the concentration of PF8S and PF8A yields k_q of $(2.4 \pm 0.6)\times10^9$ M^{-1} s^{-1} and $(7.1 \pm 0.6)\times10^8$ M^{-1} s^{-1}, respectively (Table 1). To our knowledge, this is the first time a rate constant has

been reported for the reduction of PF8S by e_{aq}^- on these timescales. We will, however, note that Gu, et. al.[79] report a decrease in the lifetime of e_{aq}^- resulting from UV-irradiation of ethylenediaminetetraacetic acid in the presence of PF8S. Although the authors do not explicitly analyze their decays to give a rate constant for the reaction of e_{aq}^- + PF8S, based on the transient absorption data in their manuscript, we estimate that the rate constant is ~ $5x10^8$ M^{-1} s^{-1}. This is only a factor of ~ 5 less than what is reported here.

In addition to PF8S and PF8A, we also studied the interaction of e_{aq}^- with PFxS and PFxA compounds of different carbon chain lengths with the resulting k_q, also reported in Table 1. We compare PFxS and PFxA in terms of the number of perfluorinated carbons they contain (e.g., PF9A and PF8S both have eight perfluorinated carbons). Comparing PF9A, $k_q = (6.4 \pm 0.4)x10^8$ M^{-1} s^{-1}, and PF8S we find that their respective k_q values are within a factor of ~ 2 (Table 1). In general, the k_q from PF2A to PF9A display no chain length dependence (Figure 13B). The same lack of a chain length dependence on k_q is also found for PFxS.

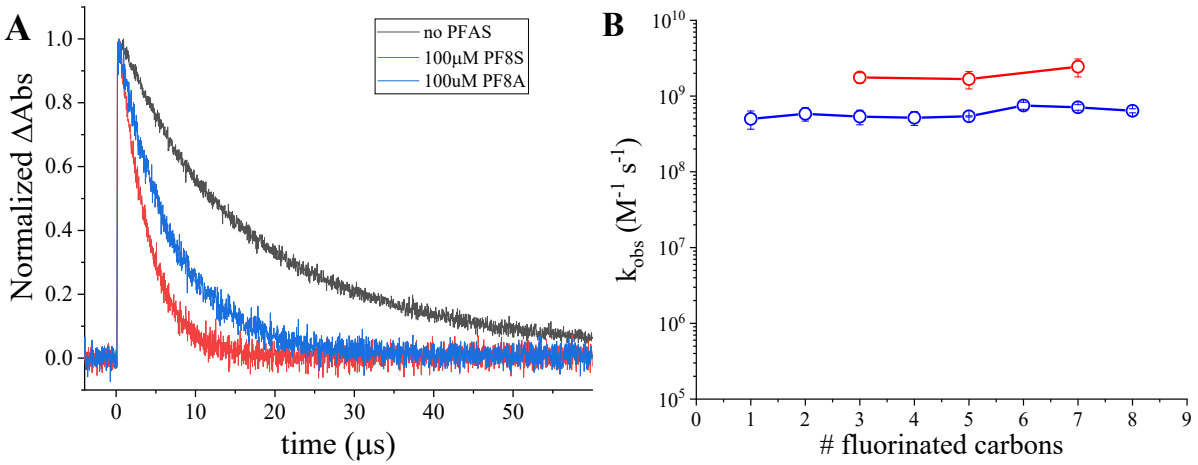

Figure 13. (Left panel) Normalized transient e_{aq}^- lifetime decays in the absence (black) and presence of 230 μM PF8S (red) and 280 μM PF8A (blue). (Right panel) Plot of the k_q for the various PFxAs (blue) and PFxSs (red) probed here as a function of the number of perfluorinated carbons in the PFAS backbone.

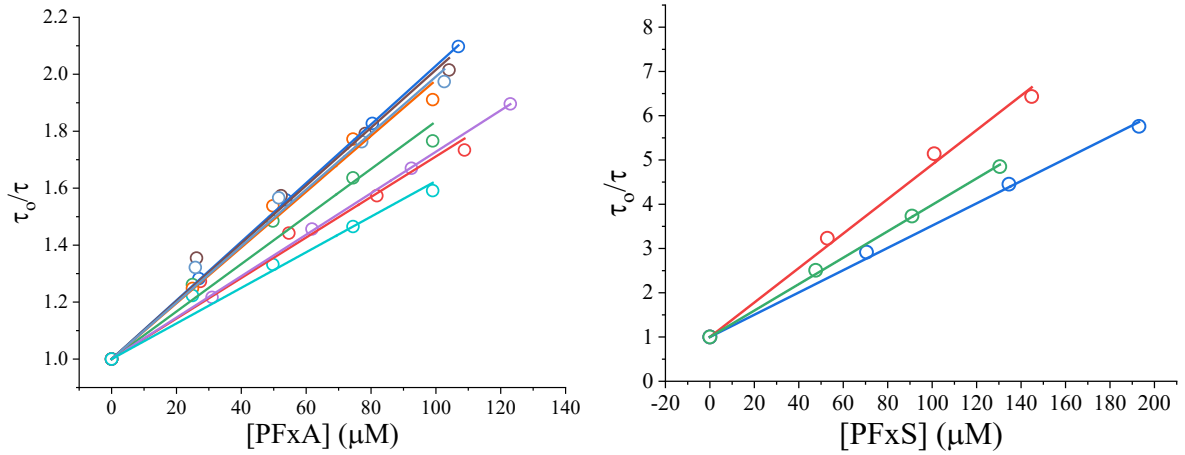

Figure 14. (Left panel) Stern-Volmer plots for the quenching of e_{aq}^- by PF9A (red), PF8A (blue), PF7A (green), PF6A (purple), PF5A (orange), PF4A (brown), PF3A (light blue), and PF2A (cyan). (Right panel) Stern-Volmer plots for the quenching of e_{aq}^- by PF8S (red), PF6S (blue), and PF4S (green).

It should be noted that the magnitude of the k_q reported here for PF8A differs from that reported by Huang, et al.[52], $k_q = (1.7 \pm 0.5)x10^7$ M^{-1} s^{-1}, by almost two orders of magnitude. The reason for this discrepancy is not immediately apparent; for the data reported here, ionic strength has a negligible effect

on the observed rate constants even at the highest concentration of PFAS probed (≤ 200 μM), where the observed and corrected rate constants differ by < 10%. We will note that based on the concentration reportedly used by Huang, et al.[52] for their first addition of trifluoroacetate, we are at least two orders of magnitude lower in concentration by our last addition of PFxA; no information was given by the authors concerning the concentration range of PF8A used in their study.

The activation energies, E_a, associated with the reaction between the e_{aq}^- and PFxA or PFxS (Figure 15 and 16) are obtained by Arrhenius analysis of the temperature dependence of k_q. Both the Φ_e and τ_o are known to be dependent on the temperature.[69, 80] Therefore, lifetime decays are obtained in the absence and presence of PFxA or PFxS in order to separate the contributions of τ_o and k_q to the overall rate of decay according to Equation **15**. An E_a of 13 ± 3 kJ mol^{-1} and 10 ± 1 kJ mol^{-1} are obtained for PF8S and PF9A, respectively, and are found to be relatively independent of the PFAS probed. Activation energies of this magnitude are consistent with most reactions involving solvated electrons and are discussed in more detail below.[61, 81-83]

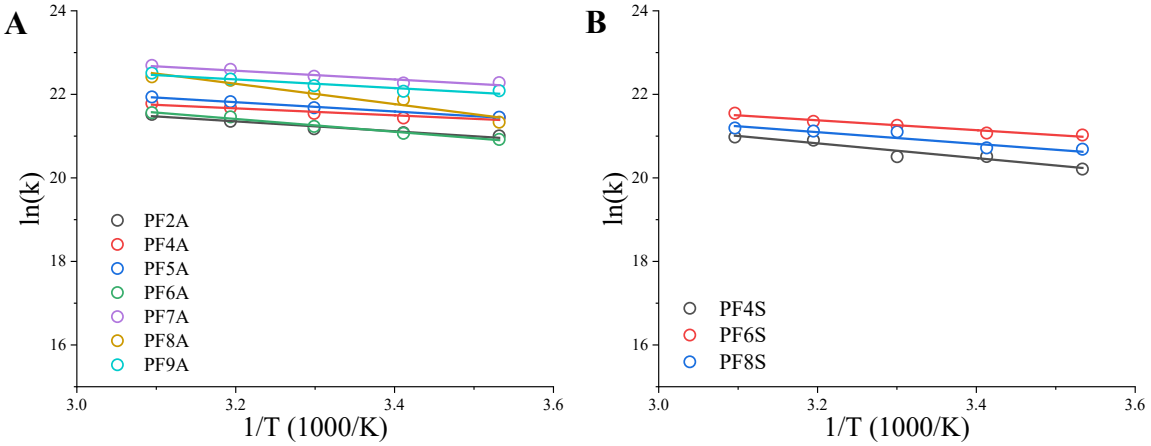

Figure 15. Arrhenius plots for the temperature dependence on the quenching rate constant, k_q, for (left panel) PFxA and (right panel) PFxS.

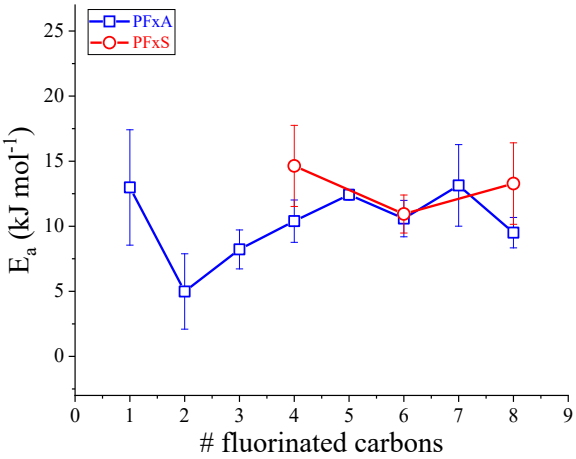

Figure 16. Activation energies for the reduction of PFxA (black squares) and PFxS (red circles) as a function of the number of fluorinated carbons comprising the fluoroalkyl backbone.

Table 1. Bimolecular quenching rate constant and activation energy for the reaction between e_{aq}^- and PFxA, PFxS.

# of fluorinated carbons	PFAS	k_q (M^{-1} s^{-1})	E_a (kJ mol^{-1})
		PFxS	
4	PF4	$(1.8 \pm 0.3)x10^9$	15 ± 3
6	PF6	$(1.7 \pm 0.4)x10^9$	11 ± 2
8	PF8	$(2.4 \pm 0.6)x10^9$	13 ± 3
		PFxA	
1	PF2	$(5.0 \pm 1.4)x10^8$	13 ± 5
2	PF3	$(5.8 \pm 1.2)x10^8$	5 ± 3
3	PF4	$(5.4 \pm 1.2)x10^8$	8 ± 2
4	PF5	$(5.2 \pm 1.1)x10^8$	10 ± 2
5	PF6	$(5.4 \pm 0.1)x10^8$	12 ± 1
6	PF7	$(7.5 \pm 0.8)x10^8$	11 ± 1
7	PF8	$(7.1 \pm 0.6)x10^8$	13 ± 3
8	PF9	$(6.4 \pm 0.4)x10^8$	10 ± 1

Arrhenius analysis of the temperature dependence of the quenching rate constant, k_q, for the PFxS and PFxA compounds revealed that the E_a associated with the reaction $e_{aq}^- + PFAS \rightarrow PFAS^-$ is on average 11 ± 3 kJ mol^{-1}, which is in good agreement with typical E_a for reactions $e_{aq}^- + A \rightarrow A^-$, where A is an electron acceptor.[84] The E_a for these types of reactions is generally independent of the reactivity (i.e. the magnitude of the $k_q(T)$) and have been assigned as being diffusion limited and, therefore, effectively barrierless.[81, 83]

van Hoomissen and Vyas[40], using DFT and natural bond orbital analysis, have calculated the VAE and AEA for a number of PFxA and PFxS of varying chain length. They found that both VAE and AEA values are consistent with the differences in the rate of reduction of PFxA vs PFxS as their predicted redox potentials differ by ~ 0.5 V. The reaction rate is expected to depend on the redox potentials of the PFAS and e_{aq}^-, as predicted by the Marcus theory of electron transfer[37], and is therefore related to the probability of PFAS reduction by e_{aq}^-. Therefore, if the point of PFAS reduction is somewhere along the interior of the PFxA carbon chain, as suggested by Bentel et al.[30] may be possible, then there should be a strong chain length dependence on the k_q, as the C-F bond dissociation energies of the interior carbons decrease with increasing chain length, presumably due to inductive effects. On the other hand, based on the theoretical data reported by van Hoomisen and Vyas[40] the k_q for reduction of the α-carbons (i.e. the carbon nearest to the acid headgroup of the surfactant), for both PFxA and PFxS, is expected to be independent of chain length. Our data suggest the latter mechanism to be the initial mode of reduction if, indeed, the AEA is an appropriate predictor of reaction rate for the first reduction reaction; that is, the initial point of electron attachment is the α-carbon adjacent to the anionic head group for both PFxA and PFxS. We carefully note, however, that we have no corroborating spectroscopic evidence. The ~ 2-fold decrease in k_q for PFxA relative to PFxS, on average, may be the result of the differences in the electron withdrawing nature of the head group.[85] It is well known that reactivity between e_{aq}^- and an electron acceptor is dependent on the relative electron deficiency of the acceptor and can be heavily influenced by the nature of substituents present on the acceptor.[85-89]

A marked chain length dependence on the overall degradation process of PFxS and no chain length dependence on the rate of degradation for PFxA for $x > 4$ have previously been reported.[30, 33] However, the lack of a chain length dependence observed here for the *initial reduction step* of PFxS and PFxA suggests that these previously observed differences in the rates of PFAS degradation between PFxS and PFxA are

rate-limited somewhere downstream in the reaction pathway. The small 2-fold increase in the k_q of PFxS relative to PFxA for the initial reduction of the linear PFASs studied here is suggestive that the initial reduction for these species occurs via a similar mechanism and their overall degradative pathways likely diverge in subsequent steps.

Currently there are two modes of thought with regard to the initial steps involved in the degradation of perfluoroalkyl carboxylates or perfluoroalkyl sulfonates by solvated electrons: either 1) defluorination (i.e., C-F bond breaking), or 2) chain shortening (i.e., C-C bond breaking).[31] The implication is that these processes occur concomitantly with PFAS reduction so that the apparent rate constant of 10^8 - 10^9 M^{-1} s^{-1} would include terms for both reduction and bond-breaking (be it C-F or C-C). We posit that based on the magnitude of the E_a obtained here for the reaction between e_{aq}- and PFAS, the two processes, reduction and bond-breaking, are de-coupled. However, it is clear that more experimental and theoretical work needs to be done to unambiguously identify and characterize the species resulting from the initial reduction of PFxA and PFxS.

5. CONCLUSIONS

The data presented in this report indicate that Zr-MOFs are capable of effectively removing anionic contaminants from aqueous media. In particular, the newly synthesized catZrMOF-1 demonstrates a capacity for PFOS that exceeds GAC. Based on UV-visible absorbance data, we propose that the adsorption of the anionic dye Eosin Y, and by extension the PFAS perfluorooctanesulfonate (PFOS), occurs by a ligand exchange mechanism where the anionic contaminant displaces a coordinated ligand from the MOF back, occupying the newly formed coordination site on the metal node of the MOF. Although the exchange of one contaminant for another by this ligand exchange mechanism proves MOFs, as a general class, as a poor choice for water treatment applications from a remediation perspective vis-à-vis degradative technologies, given the recalcitrance of PFASs compared to simple organic molecules, there is an incremental benefit to the use of MOFs in removing PFAS.

We have also shown that e_{aq}^- produced from SO_3^{2-} or $Fe(CN)_6^{4-}$ readily reacts with PFOS with a rate constant of ~ $2x10^9$ M^{-1} s^{-1}. We propose that this reaction between e_{aq}^- and PFOS results in the reduction of PFOS which is an important and necessary intermediate in the PFOS degradative pathway initiated by hydrated electrons. However, the reaction between e_{aq}^- and PFOS, or other target contaminant, is often competitively inhibited by the presence of weak acids that form at pH values between pH 10 and pH 5. Nanosecond transient absorption spectroscopy provides good evidence that in the absence of weak Brönsted acids the lifetime of e_{aq}^-, formed by photodetachment remains unperturbed down to pH ~5 providing useful insight for the design and discovery of new, more efficient, homogeneous and/or heterogeneous sources of solvated electrons.

REFERENCES

1. C. D. Vecitis, H. Park, J. Cheng, B. T. Mader and M. R. Hoffmann, Treatment Technologies for Aqueous Perfluorooctanesulfonate (PFOS) and Perfluorooctanoate (PFOA), *Front Environ Sci En*, 2009, **3**, 129-151.
2. E. M. Sunderland, X. D. C. Hu, C. Dassuncao, A. K. Tokranov, C. C. Wagner and J. G. Allen, A Review of the Pathways of Human Exposure to Poly- and Perfluoroalkyl Substances (PFASs) and Present Understanding of Health Effects, *J Expo Sci Env Epid*, 2019, **29**, 131-147.
3. P. Grandjean and R. Clapp, Perfluorinated Alkyl Substances: Emerging Insights Into Health Risks, *NEW SOLUTIONS: A Journal of Environmental and Occupational Health Policy*, 2015, **25**, 147-163.

4. G. Goldenman, M. Fernandes, M. Holland, T. Tugran, A. Nordin, C. Schoumacher and A. McNeill, *The Cost of Inaction: A Socioeconomic Analysis of Environmental and Health Impacts Linked to Exposure to PFAS*, Nordic Council of Ministers, 2019.
5. J. L. Domingo and M. Nadal, Human Exposure to Per-and Polyfluoroalkyl Substances (PFAS) Through Drinking Water: A Review of the Recent Scientific Literature, *Environ Res*, 2019, **177**.
6. B. Ji, P. Y. Kang, T. Wei and Y. Q. Zhao, Challenges of Aqueous Per- and Polyfluoroalkyl Substances (PFASs) and Their Foreseeable Removal Strategies, *Chemosphere*, 2020, **250**.
7. I. Ross, J. McDonough, J. Miles, P. Storch, P. Thelakkat Kochunarayanan, E. Kalve, J. Hurst, S. S. Dasgupta and J. Burdick, A Review of Emerging Technologies for Remediation of PFASs, *Remediation J.*, 2018, **28**, 101-126.
8. G. W. Peterson, J. Mahle, A. Balboa, G. Wagner, T. Sewell and C. J. Karwacki, *Evaluation of MOF-74, MOF-177, and ZIF-8 for the Removal of Toxic Industrial Chemicals*, EDGEWOOD CHEMICAL BIOLOGICAL CENTER ABERDEEN PROVING GROUND MD RESEARCH AND …, 2008.
9. T. Islamoglu, Z. Chen, M. C. Wasson, C. T. Buru, K. O. Kirlikovali, U. Afrin, M. R. Mian and O. K. Farha, Metal–Organic Frameworks Against Toxic Chemicals, *Chemical reviews*, 2020, **120**, 8130-8160.
10. N. S. Bobbitt, M. L. Mendonca, A. J. Howarth, T. Islamoglu, J. T. Hupp, O. K. Farha and R. Q. Snurr, Metal–Organic Frameworks for the Removal of Toxic Industrial Chemicals and Chemical Warfare Agents, *Chemical Society Reviews*, 2017, **46**, 3357-3385.
11. G. W. Peterson, T. Glover, B. J. Schindler, D. Britt and O. Yaghi, *Toxic Industrial Chemical Removal by Isostructural Metal-Organic Frameworks*, EDGEWOOD CHEMICAL BIOLOGICAL CENTER ABERDEEN PROVING GROUND MD, 2011.
12. M. Eddaoudi, J. Kim, N. Rosi, D. Vodak, J. Wachter, M. O'Keeffe and O. M. Yaghi, Systematic Design of Pore Size and Functionality in Isoreticular MOFs and Their Application in Methane Storage, *Science*, 2002, **295**, 469-472.
13. D. Feng, Z. Y. Gu, J. R. Li, H. L. Jiang, Z. Wei and H. C. Zhou, Zirconium-Metalloporphyrin PCN-222: Mesoporous Metal–Organic Frameworks with Ultrahigh Stability as Biomimetic Catalysts, *Angew. Chem. Int. Ed.*, 2012, **51**, 10307-10310.
14. P. Li, Q. Chen, T. C. Wang, N. A. Vermeulen, B. L. Mehdi, A. Dohnalkova, N. D. Browning, D. Shen, R. Anderson and D. A. Gómez-Gualdrón, Hierarchically engineered mesoporous metal-organic frameworks toward cell-free immobilized enzyme systems, *Chem*, 2018, **4**, 1022-1034.
15. P. S. Pauletto and T. J. Bandosz, Activated Carbon versus Metal-Organic Frameworks: A Review of Their PFAS Adsorption Performance, *J Hazard Mater*, 2022, **425**.
16. R. Li, S. Alomari, T. Islamoglu, O. K. Farha, S. Fernando, S. M. Thagard, T. M. Holsen and M. Wriedt, Systematic Study on the Removal of Per-and Polyfluoroalkyl Substances from Contaminated Groundwater Using Metal–Organic Frameworks, *Environ Sci Technol*, 2021, **55**, 15162-15171.
17. R. Li, S. Alomari, R. Stanton, M. C. Wasson, T. Islamoglu, O. K. Farha, T. M. Holsen, S. M. Thagard, D. J. Trivedi and M. Wriedt, Efficient Removal of Per-and Polyfluoroalkyl Substances from Water with Zirconium-Based Metal–Organic Frameworks, *Chem Mater*, 2021, **33**, 3276-3285.
18. D. Barpaga, J. Zheng, K. S. Han, J. A. Soltis, V. Shutthanandan, S. Basuray, B. P. McGrail, S. Chatterjee and R. K. Motkuri, Probing the Sorption of Perfluorooctanesulfonate Using Mesoporous Metal–Organic Frameworks from Aqueous Solutions, *Inorg Chem*, 2019, **58**, 8339-8346.
19. R. Li, S. Alomari, T. Islamoglu, O. K. Farha, S. Fernando, S. M. Thagard, T. M. Holsen and M. Wriedt, Systematic Study on the Removal of Per- and Polyfluoroalkyl Substances from Contaminated Groundwater Using Metal-Organic Frameworks, *Environ Sci Technol*, 2021, **55**, 15162-15171.

20. B. P. Vellanki, B. Batchelor and A. Abdel-Wahab, Advanced Reduction Processes: A New Class of Treatment Processes, *Environ Eng Sci*, 2013, **30**, 264-271.
21. S. Y. Yang, Y. T. Zhang and D. Zheng, Advanced Reduction Processes: A Novel Technology for Water Treatment, *Prog Chem*, 2016, **28**, 934-941.
22. M. H. Cao, B. B. Wang, H. S. Yu, L. L. Wang, S. H. Yuan and J. Chen, Photochemical Decomposition of Perfluorooctanoic Acid in Aqueous Periodate with VUV and UV Light Irradiation, *J Hazard Mater*, 2010, **179**, 1143-1146.
23. Y. R. Gu, W. Y. Dong, C. Luo and T. Z. Liu, Efficient Reductive Decomposition of Perfluorooctanesulfonate in a High Photon Flux UV/Sulfite System, *Environ Sci Technol*, 2016, **50**, 10554-10561.
24. Y. R. Gu, T. Z. Liu, H. J. Wang, H. L. Han and W. Y. Dong, Hydrated Electron Based Decomposition of Perfluorooctane Sulfonate (PFOS) in the VUV/Sulfite System, *Sci Total Environ*, 2017, **607**, 541-548.
25. L. Jin and P. Zhang, Photochemical Decomposition of Perfluorooctane Sulfonate (PFOS) in an Anoxic Alkaline Solution by 185 nm Vacuum Ultraviolet, *Chem Eng J*, 2015, **280**, 241-247.
26. V. Ochoa-Herrera, R. Sierra-Alvarez, A. Somogyi, N. E. Jacobsen, V. H. Wysocki and J. A. Field, Reductive Defluorination of Perfluorooctane Sulfonate, *Environ Sci Technol*, 2008, **42**, 3260-3264.
27. H. Park, C. D. Vecitis, J. Cheng, N. F. Dalleska, B. T. Mader and M. R. Hoffmann, Reductive Degradation of Perfluoroalkyl Compounds with Aquated Electrons Generated from Iodide Photolysis at 254 nm, *Photoch Photobio Sci*, 2011, **10**, 1945-1953.
28. Y. Qu, C. J. Zhang, F. Li, J. Chen and Q. Zhou, Photo-Reductive Defluorination of Perfluorooctanoic Acid in Water, *Water Res*, 2010, **44**, 2939-2947.
29. Z. Song, H. Q. Tang, N. Wang and L. H. Zhu, Reductive Defluorination of Perfluorooctanoic Acid by Hydrated Electrons in a Sulfite-Mediated UV Photochemical System, *J Hazard Mater*, 2013, **262**, 332-338.
30. M. J. Bentel, Y. Yu, L. Xu, Z. Li, B. M. Wong, Y. Men and J. Liu, Defluorination of Per- and Polyfluoroalkyl Substances (PFASs) with Hydrated Electrons: Structural Dependence and Implications to PFAS Remediation and Management, *Environ Sci Technol*, 2019, **53**, 3718-3728.
31. J. K. Cui, P. P. Gao and Y. Deng, Destruction of Per- and Polyfluoroalkyl Substances (PFAS) with Advanced Reduction Processes (ARPs): A Critical Review, *Environ Sci Technol*, 2020, **54**, 3752-3766.
32. H. F. Schroder and R. J. W. Meesters, Stability of Fluorinated Surfactants in Advanced Oxidation Processes - A Follow Up of Degradation Products Using Flow Injection-Mass Spectrometry, Liquid Chromatography-Mass Spectrometry and Liquid Chromatography-Multiple Stage Mass Spectrometry, *J Chromatogr A*, 2005, **1082**, 110-119.
33. H. Park, C. D. Vecitis, J. Cheng, W. Choi, B. T. Mader and M. R. Hoffmann, Reductive Defluorination of Aqueous Perfluorinated Alkyl Surfactants: Effects of Ionic Headgroup and Chain Length, *J Phys Chem A*, 2009, **113**, 690-696.
34. X. Li, J. Fang, G. Liu, S. Zhang, B. Pan and J. Ma, Kinetics and Efficiency of the Hydrated Electron-Induced Dehalogenation by the Sulfite/UV Process, *Water Res*, 2014, **62**, 220-228.
35. Y. R. Gu, T. Z. Liu, Q. Zhang and W. Y. Dong, Efficient Decomposition of Perfluorooctanoic Acid by a High Photon Flux UV/Sulfite Process: Kinetics and Associated Toxicity, *Chem Eng J*, 2017, **326**, 1125-1133.
36. K. E. Yu, X. C. Li, L. W. Chen, J. Y. Fang, H. L. Chen, Q. B. Li, N. P. Chi and J. Ma, Mechanism and Efficiency of Contaminant Reduction by Hydrated Electron in the Sulfite/Iodide/UV Process, *Water Res*, 2018, **129**, 357-364.
37. R. A. Marcus, Theory of Electron-Transfer Reaction Rates of Solvated Electrons, *J. Chem. Phys.*, 1965, **43**, 3477-3489.
38. J. A. Marsella, A. G. Gilicinski, A. M. Coughlin and G. P. Pez, Selective Reduction of Saturated Perfluorocarbons, *J Org Chem*, 1992, **57**, 2856-2860.

39. A. A. Pud, G. S. Shapoval, V. P. Kukhar, O. E. Mikulina and L. L. Gervits, Electrochemical Reduction of Some Saturated and Unsaturated Perfluorocarbons, *Electrochim Acta*, 1995, **40**, 1157-1164.
40. D. J. Van Hoomissen and S. Vyas, Early Events in the Reductive Dehalogenation of Linear Perfluoroalkyl Substances, *Environ. Sci. Technol. Lett.*, 2019, **6**, 365-371.
41. B. Guan, J. Zhi, X. Zhang, T. Murakami and A. Fujishima, Electrochemical Route for Fluorinated Modification of Boron-Doped Diamond Surface with Perfluorooctanoic Acid, *Electrochem Commun*, 2007, **9**, 2817-2821.
42. W. A. Maza, V. M. Breslin, N. T. Plymale, P. A. DeSario, A. Epshteyn, J. C. Owrutsky and B. B. Pate, Nanosecond Transient Absorption Studies of the pH-Dependent Hydrated Electron Quenching by HSO_3^-, *Photoch Photobio Sci*, 2019, **18**, 1526-1532.
43. R. Li, S. Alomari, R. Stanton, M. C. Wasson, T. Islamoglu, O. K. Farha, T. M. Holsen, S. M. Thagard, D. J. Trivedi and M. Wriedt, Efficient Removal of Per- and Polyfluoroalkyl Substances from Water with Zirconium-Based Metal-Organic Frameworks, *Chem Mater*, 2021, **33**, 3276-3285.
44. A. E. Martell and R. M. Smith, *Critical Stability Constants*, Plenum Press, New York, N.Y., 1974.
45. E. Hayon, A. Treinin and J. Wilf, Electronic Spectra, Photochemistry, and Autoxidation Mechanism of Sulfite-Bisulfite-Pyrosulfite Systems - SO_2^-, SO_3^-, SO_4^-, and SO_5^- Radicals, *J Am Chem Soc*, 1972, **94**, 47-57.
46. L. Dogliotti and E. Hayon, Flash Photolysis Study of Sulfite, Thiocyanate, and Thiosulfate Ions in Solution, *J Phys Chem*, 1968, **72**, 1800-1807.
47. M. C. Sauer, R. A. Crowell and I. A. Shkrob, Electron Photodetachment from Aqueous Anions. 1. Quantum Yields for Generation of Hydrated Electron by 193 and 248 nm Laser Photoexcitation of Miscellaneous Inorganic Anions, *J. Phys. Chem. A.*, 2004, **108**, 5490-5502.
48. G. M. Sando and J. C. Owrutsky, Photodetachment of Ferrocyanide in Reverse Micelles, *J Phys Chem B*, 2006, **110**, 9586-9592.
49. G. Stein, Photochemistry of the Ferrocyanide Ion in Aqueous Solution: Hydrated Electron Formation and Aquation, *Isr. J. Chem.*, 1970, **8**, 691-697.
50. P. Airey and F. S. Dainton, The photochemistry of aqueous solutions of Fe (II) II. Processes in acidified solutions of potassium ferrocyanide at 25° C, *Proc. R. Soc. Lond. A*, 1966, **291**, 478-486.
51. S. S. R. K. C. Yamijala, R. Shinde and B. M. Wong, Real-Time Degradation Dynamics of Hydrated Per- and Polyfluoroalkyl Substances (PFASs) in the Presence of Excess Electrons, *Physical Chemistry Chemical Physics*, 2020, **22**, 6804-6808.
52. L. Huang, W. B. Dong and H. Q. Hou, Investigation of the Reactivity of Hydrated Electron Toward Perfluorinated Carboxylates by Laser Flash Photolysis, *Chem. Phys. Lett.*, 2007, **436**, 124-128.
53. L. Robertson and R. C. Hartley, Synthesis of N-arylpyridinium salts bearing a nitrone spin trap as potential mitochondria-targeted antioxidants, *Tetrahedron*, 2009, **65**, 5284-5292.
54. Q. Sui, X. T. Ren, Y. X. Dai, K. Wang, W. T. Li, T. Gong, J. J. Fang, B. Zou, E. Q. Gao and L. Wang, Piezochromism and Hydrochromism Through Electron Transfer: New Stories for Viologen Materials, *Chem Sci*, 2017, **8**, 2758-2768.
55. Q. Y. Yang, V. Guillerm, F. Ragon, A. D. Wiersum, P. L. Llewellyn, C. L. Zhong, T. Devic, C. Serre and G. Maurin, CH4 storage and CO2 capture in highly porous zirconium oxide based metal-organic frameworks, *Chemical communications*, 2012, **48**, 9831-9833.
56. A. Schaate, P. Roy, T. Preuße, S. J. Lohmeier, A. Godt and P. Behrens, Porous Interpenetrated Zirconium–Organic Frameworks (PIZOFs): A Chemically Versatile Family of Metal–Organic Frameworks, *Chemistry–A European Journal*, 2011, **17**, 9320-9325.

57. S. Lath, E. R. Knight, D. A. Navarro, R. S. Kookana and M. J. McLaughlin, Sorption of PFOA onto Different Laboratory Materials: Filter Membranes and Centrifuge Tubes, *Chemosphere*, 2019, **222**, 671-678.
58. G. V. Buxton, C. L. Greenstock, W. P. Helman and A. B. Ross, Critical-Review of Rate Constants for Reactions of Hydrated Electrons, Hydrogen-Atoms and Hydroxyl Radicals ($^{\cdot}OH/^{\cdot}O^{-}$) in Aqueous-Solution, *J Phys Chem Ref Data*, 1988, **17**, 513-886.
59. L. M. Dorfman, F. Jou and R. Wageman, Solvated Electron Solvent Dependence of the Optical Absorption Spectrum of the Solvated Electron, *Berich Bunsen Gesell*, 1971, **75**, 681-685.
60. E. J. Hart, B. Michael and K. H. Schmidt, Absorption Spectrum of e_{aq}^{-} in the Temperature Range -4 to 390°, *The Journal of Physical Chemistry*, 1971, **75**, 2798-2805.
61. B. Čerček, Effect of Structure of Water on Activation Energies of Reactions of Hydrated Electron. 1. Effects of Aliphatic Alcohols, $MgCl_2$ and KI as Co-Solutes, *Int J Radiat Phys Ch*, 1971, **3**, 231-&.
62. M. Anbar, M. Bambenek and A. B. Ross, *Selected Specific Rates of Reactions of Transients from Water in Aqueous Solution*, U.S. National Bureau of Standards, Washington, D.C., 1973.
63. P. Airey and F. S. Dainton, The Photochemistry of Aqueous Solutions of Fe(II) II. Processes in Acidified Solutions of Potassium Ferrocyanide at 25° C, *Proc. R. Soc. Lond. A*, 1966, **291**, 478-486.
64. G. Czapski and H. A. Schwarz, The Nature of the Reducing Radical in Water Radiolysis, *The Journal of Physical Chemistry*, 1962, **66**, 471-474.
65. S. Gordon, E. J. Hart, M. S. Matheson, J. Rabani and J. K. Thomas, Reaction Constants of the Hydrated Electron, *J Am Chem Soc*, 1963, **85**, 1375-1377.
66. J. Rabani, On the Reactivity of Hydrogen Atoms in Aqueous Solution, *The Journal of Physical Chemistry*, 1962, **66**, 361-362.
67. M. Shirom and G. Stein, Excited State Chemistry of the Ferrocyanide Ion in Aqueous Solution. II. Photoaquation, *The Journal of Chemical Physics*, 1971, **55**, 3379-3382.
68. M. Reinhard, G. Auböck, N. A. Besley, I. P. Clark, G. M. Greetham, M. W. Hanson-Heine, R. Horvath, T. S. Murphy, T. J. Penfold and M. Towrie, Photoaquation Mechanism of Hexacyanoferrate(II) Ions: Ultrafast 2D UV and Transient Visible and IR Spectroscopies, *J Am Chem Soc*, 2017, **139**, 7335-7347.
69. C. D. Borsarelli, S. G. Bertolotti and C. M. Previtali, Thermodynamic Changes Associated with the Formation of the Hydrated Electron After Photoionization of Inorganic Anions: A Time-Resolved Photoacoustic Study, *Photoch Photobio Sci*, 2003, **2**, 791-795.
70. M. Shirom and G. Stein, Excited State Chemistry of the Ferrocyanide Ion in Aqueous Solution. I. Formation of the Hydrated Electron, *J. Chem. Phys.*, 1971, **55**, 3372-3378.
71. M. Lewis and C. Jonah, Evidence for Two Electron States in Solvation and Scavenging Processes in Alcohols, *The Journal of Physical Chemistry*, 1986, **90**, 5367-5372.
72. H. Ghosh, D. Palit, A. Sapre, K. RamaRao and J. Mittal, Dual Sites of Solvation for Electrons Produced by Photoionisation in Aqueous Micellar Solutions, *Chem. Phys. Lett.*, 1993, **203**, 5-11.
73. M. S. Matheson, W. Mulac and J. Rabani, Formation of the Hydrated Electron in the Flash Photolysis of Aqueous Solutions, *The Journal of Physical Chemistry*, 1963, **67**, 2613-2617.
74. E. M. Fielden and E. J. Hart, Activation Energy of Hydrated Electron+Water Reaction and Ultra-Violet Absorption Spectrum of Hydrated Electron, *Trans Faraday Soc*, 1967, **63**, 2975-2982.
75. M. Shirom and Tomkiewi.M, Quantum Yield of Solvated Electrons from Ferrocyanide in Various Water-Alcohol Mixtures, *J. Chem. Phys.*, 1972, **56**, 2731-&.
76. L. M. Dorfman, F. Jou and R. Wageman, Solvent Dependence of the Optical Absorption Spectrum of the solvated Electron, *Berich Bunsen Gesell*, 1971, **75**, 681-685.
77. E. J. Hart and J. W. Boag, Absorption Spectrum of the Hydrated Electron in Water and in Aqueous Solutions, *J Am Chem Soc*, 1962, **84**, 4090-4095.
78. M. A. Rodgers, D. C. Foyt and Z. A. Zimek, The Effect of Surfactant Micelles on the Reaction between Hydrated Electrons and Dimethyl Viologen, *Radiation Research*, 1978, **75**, 296-304.

79. P. F. Gu, C. J. Zhang, Z. Y. Sun, H. Z. Zhang, Q. Zhou, S. J. Lin, J. Y. Rong and M. R. Hoffmann, Enhanced Photoreductive Degradation of Perfluorooctanesulfonate by UV Irradiation in the Presence of Ethylenediaminetetraacetic Acid, *Chem Eng J*, 2020, **379**.
80. N. Chandrasekhar and P. Krebs, The Spectra and the Relative Yield of Solvated Electrons Produced by Resonant Photodetachment of Iodide Anion in Ethylene Glycol in the Temperature Range $296 \leq T \leq 453$ K, *J Chem Phys*, 2000, **112**, 5910-5914.
81. B. Čerček, Activation Energies for Reactions of Hydrated Electron, *Nature*, 1969, **223**, 491-&.
82. B. Čerček, Effect of the Structure of Water on the Activation Energies of Reactions of the Hydrated Electron—I: Effects of Aliphatic Alcohols, $MgCl_2$ and Kl as Co-Solutes, *Int J Radiat Phys Ch*, 1971, **3**, 231-237.
83. B. Čerček and M. Ebert, Activation Energies for Reactions of Hydrated Electron, *J Phys Chem*, 1968, **72**, 766-766.
84. M. Anbar and E. J. Hart, Activation Energy of Hydrated Electron Reactions, *The Journal of Physical Chemistry*, 1967, **71**, 3700-3702.
85. M. Anbar and E. J. Hart, The Reactivity of Aromatic Compounds toward Hydrated Electrons, *J Am Chem Soc*, 1964, **86**, 5633-5637.
86. M. Anbar, in *Solvated Electron*, ed. R. F. Gould, American Chemical Society, Washington, D.C., 1965, vol. 50, ch. 6, pp. 55-81.
87. M. Anbar, in *Advances in Physical Organic Chemistry*, ed. V. Gold, Academic Press, London, 1969, vol. 7, pp. 115-151.
88. M. Anbar, Z. B. Alfassi and Bregmanr.H, Hydrated Electron Reactions in View of Their Temperature Dependence, *J Am Chem Soc*, 1967, **89**, 1263-1264.
89. M. Anbar and E. J. Hart, The Reaction of Haloaliphatic Compounds with Hydrated Electrons, *The Journal of Physical Chemistry*, 1965, **69**, 271-274.